Acknowledgment. This research was supported by the NSF through the Northwestern Materials Research Center (Grant DMR 8520280) and by the Office of Naval Research.

Registry No. TOS^-, 16722-51-3; PYS^-, 90792-23-7; $NFBS^-$, 45187-15-3; $PFOS^-$, 45298-90-6; $[Si(Pc)O]_n$, 39114-20-0; γ-Ni(Pc), 14055-02-8; $[(n\text{-}Bu_4N^+)PYS^-]$, 120386-01-8; $[(n\text{-}Bu_4N^+)PF_6^-]$, 3109-63-5; $[(n\text{-}Bu_4N^+)SbF_6^-]$, 22505-58-4; $[(n\text{-}Bu_4N^+)CF_3SO_3^-]$, 35895-70-6; $[(n\text{-}Bu_4N^+)NFBS^-]$, 102091-92-9; $[(Et_4N^+)PFOS^-]$, 56773-42-3; $[(n\text{-}Bu_4N^+)_2SO_4^{2-}]$, 2472-88-0; $[(n\text{-}Bu_4N^+)BF_4^-]$, 429-42-5; $[(Et_4N^+)TOS^-]$, 733-44-8; $[Ge(Pc)O]_n$, 55948-70-4; BF_4^-, 14874-70-5; PF_6^-, 16919-18-9; SbF_6^-, 17111-95-4; $CF_3SO_3^-$, 37181-39-8; SO_4^{2-}, 14808-79-8.

Supplementary Material Available: X-ray diffraction data for polycrystalline $\{[Si(Pc)O](TOS)_{0.85}\}_n$ (1 page). Ordering information is given on any current masthead page.

Molecular Metals with Widely Tunable Band Filling. Response of the Collective Properties of a Phthalocyanine Molecular Metal to Drastic Excursions in Partial Oxidation State and Charge-Compensating Counterions

Manuel Almeida,[1a] John G. Gaudiello,[1a] Glen E. Kellogg,[1a] Stephen M. Tetrick,[1a] Henry O. Marcy,[1b] William J. McCarthy,[1b] John C. Butler,[1b] Carl R. Kannewurf,[1b] and Tobin J. Marks*,[1a]

Contribution from the Department of Chemistry, the Department of Electrical Engineering and Computer Science, and the Materials Research Center, Northwestern University, Evanston, Illinois 60208. *Received July 18, 1988*

Abstract: The electrical, optical, and magnetic properties of the partially oxidized, cofacially joined phthalocyanine polymers $\{[Si(Pc)O]X_y\}_n$ are investigated for $X^- = BF_4^-$, $y = 0.00$–0.50; X^- = *p*-toluenesulfonate (TOS^-), $y = 0.00$–0.67; and $X^- = SO_4^{2-}$, $y = 0.040$, 0.095. As a function of increasing y, the physical properties of the BF_4^- and TOS^- salts evidence a transition at $y \approx 0.20$ from a localized carrier semiconductor or insulator to a molecular metal. Thus, the dc electrical conductivity increases from low values having a temperature dependence most characteristic of disorder and/or hopping transport between localized states to values characteristic of a molecular metal with fluctuation-induced carrier tunneling between relatively large metallike particles. Beyond $y \gtrsim 0.25$, the conductivity is only weakly dependent on y. At $y \approx 0.20$, the thermoelectric power $[S(T)]$ also changes from behavior characteristic of a p-type semiconductor or insulator to that of a p-type molecular metal. Differences in $S(T)$ between $X^- = BF_4^-$ and TOS^- polymers appear to be due largely to minor structural variations. Optical reflectivity measurements reveal the appearance of a metallike plasma edge at $y \approx 0.20$, followed by an incremental shift of this feature to higher energy with further increase in y. The static magnetic susceptibility of $\{[Si(Pc)O](BF_4)_y\}_n$ evidences an abrupt transition at $y \approx 0.20$ from a large concentration of localized, Curie-like spins to Pauli-like behavior characteristic of a molecular metal. Beyond $y \gtrsim 0.30$, the Pauli-like susceptibility is nearly independent of y. ESR studies indicate a ligand-centered π-radical-cation electronic structure. For $X^- = BF_4^-$ and TOS^-, line-width studies as a function of y evidence a progression from relatively localized to delocalized carriers. It is suggested that the insulator/semiconductor to molecular metal transition in these materials is an Anderson-like transition that arises when the Fermi level crosses a mobility edge from localized states (presumably due to disorder and/or defects) at the tail of the conduction band to delocalized, metallike states. With the possible exception of ESR line-width data, the electrical, optical, and magnetic studies of $\{[Si(Pc)O](SO_4)_{0.095}\}_n$ provide no evidence for an enhanced, carrier-localizing perturbation of the $[Si(Pc^{\rho+})O]_n$ band structure by the dinegative off-axis counterions.

In the preceding contribution,[2] we discussed chemical, structural, and thermodynamic aspects of electrochemically oxidizing ("doping") the cofacially joined metallophthalocyanine polymer $[Si(Pc)O]_n$ to yield products of the type $\{[Si(Pc)O]X_y\}_n$. Under conditions in which molecular stacking is rigorously enforced, it was shown to be possible not only to effect significant variation in X^-, but also to achieve wide and continuous tuning of the conduction band filling, $(2 - y)/2$. Such counterion and band-filling tunability with invariant stacking has not previously been achievable to any major extent for any conventional molecular conductor.[3] Since partially oxidized stacked molecular metallophthalocyanines form the basis for a broad class of predominantly ligand-centered molecular metals,[4,5] it was of great interest to learn how the collective properties of a stacking-enforced, metallike phthalocyanine assembly would respond to the tuning of such perturbations.

We report here a combined charge-transport (variable-temperature conductivity and thermoelectric power), optical spectroscopic, and magnetic investigation of the $\{[Si(Pc)O]X_y\}_n$ system for both a small, nonpolarizable counterion ($X^- = BF_4^-$, $y = 0$–0.50), and a large, polarizable, aromatic counterion (X^- =

(1) (a) Department of Chemistry and the Materials Research Center. (b) Department of Electrical Engineering and Computer Science and the Materials Research Center.

(2) Gaudiello, J. G.; Kellogg, G. E.; Tetrick, S. M.; Marks, T. J. *J. Am. Chem. Soc.*, preceding paper in this issue.

(3) (a) *Proc. Int. Conf. Sci. Technol. Synth. Met. Synth. Met.* **1987**, *17–19*. (b) Jérome, D., Caron, L. G., Eds. *Low-Dimensional Conductors and Superconductors*; Plenum: New York, 1987. (c) Ferraro, J. R.; Williams, J. M. *Introduction to Synthetic Electrical Conductors*; Academic Press: New York, 1987. (d) Becker, J. Y., Bernstein, J., Bittner, S., Eds. *Isr. J. Chem.* **1986**, *27*(4). (e) Cowan, D. O.; Wiygul, F. M. *Chem. Eng. News* **1986**, *64*, 28–45. (f) Cohen, M. L. *Science* **1986**, *234*, 549–553. (g) Williams, J. M. *Prog. Inorg. Chem.* **1985**, *33*, 183–220. (h) Wudl, F. *Acc. Chem. Res.* **1984**, *17*, 227–232. (i) Greene, R. L.; Street, G. B. *Science* **1984**, *226*, 651–656. (j) Miller, J. S., Ed. *Extended Linear Chain Compounds*; Plenum: New York, 1982; Vol. 1–3.

(4) Marks, T. J. *Science* **1985**, *227*, 881–889.

(5) (a) Almeida, M.; Kanatzidis, M. G.; Tonge, L. M.; Marks, T. J.; Marcy, H. O.; McCarthy, W. J.; Kannewurf, C. R. *Solid State Commun.* **1987**, *63*, 457–461. (b) Inabe, T.; Liang, W.-B.; Lomax, J. F.; Nakamura, S.; Lyding, J. W.; McCarthy, W. J.; Carr, S. H.; Kannewurf, C. R.; Marks, T. J. *Synth. Met.* **1986**, *13*, 219–229. (c) Gaudiello, J. G.; Marcy, H. O.; McCarthy, W. J.; Moguel, M. K.; Kannewurf, C. R.; Marks, T. J. *Synth. Met.* **1986**, *15*, 115–128. (d) Inabe, T.; Nakumura, S.; Liang, W.-B.; Marks, T. J.; Burton, R. L.; Kannewurf, C. R.; Imaeda, K.-I. *J. Am. Chem. Soc.* **1985**, *107*, 7224–7226. (e) Inabe, T.; Marks, T. J.; Burton, R. L.; Lyding, J. W.; McCarthy, W. J.; Kannewurf, C. R.; Reisner, G. M.; Herbstein, F. H. *Solid State Commun.* **1985**, *54*, 501–504. (f) Martinsen, J.; Palmer, S. M.; Tanaka, J.; Greene, R. C.; Hoffman, B. M. *Phys. Rev. B* **1984**, *30*, 6269–6276. (g) Yakushi, K.; Sakuda, M.; Hamada, I.; Kuroda, H.; Kawamoto, A.; Tanaka, J.; Sugano, T.; Kinoshita, M. In ref 3a, *19*, 769–774. (h) Schramm, C. J.; Scaringe, R. P.; Stojakovic, D. R.; Hoffman, B. M.; Ibers, J. A.; Marks, T. J. *J. Am. Chem. Soc.* **1980**, *102*, 6702–6713.

0002-7863/89/1511-5271$01.50/0

p-toluenesulfonate, TOS^-, $y = 0-0.67$).[6] We also report on the properties of the first molecular metal to contain a charge-compensating dianion (SO_4^{2-}). The interest in the latter system has been to determine whether additional off-axis Coulombic attraction might effect partial or complete pinning of the phthalocyanine-centered (hole) carriers. The present results overall conform surprisingly well to some of the predictions of simple Hückel-like tight-binding band theory;[7] however, there are also notable deviations. In both $\{[Si(Pc)O](BF_4)_y\}_n$ and $\{[Si(Pc)O](TOS)_y\}_n$, metallic characteristics are not completely tunable over the full range of accessible y values. Rather, both materials exhibit an insulator-to-metal transition at $y \approx 0.2$.

Experimental Section

Materials. The $\{[Si(Pc)O]X_y\}_n$ materials used in this study ($X^- = BF_4^-$, TOS^-, SO_4^{2-}) were prepared as described in the accompanying contribution.[2] Purity was routinely monitored by elemental analysis and X-ray powder diffraction.

Static Magnetic Susceptibility Measurements. Static magnetic susceptibility measurements were performed with a S.H.E. VTS-10 SQUID susceptometer, using previously described procedures and precautions.[8] The purity of the $Si(Pc)Cl_2$ starting complex had a dramatic effect on measured susceptibilities of doped $\{[Si(Pc)O]X_y\}_n$ materials, and purification of $Si(Pc)Cl_2$ proceeded as described elsewhere.[2] The diamagnetic correction for the $[Si(Pc)O]_n$ polymer was -4.455×10^{-4} emu mol^{-1}, as reported previously.[8] The diamagnetic correction for the BF_4^- counterion (-0.422×10^{-4} emu mol^{-1}) was calculated from tabulated Pascal constants.[9] Depending upon the type of sample, Curie-like features were analyzed by χ vs $1/T$ linear regression techniques or by χ vs $T^{-\alpha}$ ($\alpha < 1$) power law regression techniques.

ESR Spectroscopy. Electron spin resonance experiments were carried out on a modified Varian E-4 X-band ESR spectrometer equipped with a 4-in. magnet and using 100-kHz field modulation. The field was calibrated with 2,2-diphenyl-1-picrylhydrazyl (DPPH, $g = 2.0036$). The cavity resonance frequency was measured with a wavemeter. Samples were examined as powders after pumping 24 h in vacuo and sealing under argon in 2-mm quartz tubes.

Reflectance Spectroscopy. Reflectance spectra of polycrystalline $\{[Si(Pc)O]X_y\}_n$ compactions were measured by using two dispersive grating instruments and a Fourier transform spectrometer. All measurements were made at room temperature and at near-normal incidence. The samples, pressed by polished dies exerting 7–10 tons of force, were disks 13 mm in diameter and 0.5–1.0 mm thick (similar to those used for the diffraction[2] and charge-transport studies). Visual examination of the pellet surfaces under 320× magnification revealed smooth, specular surfaces with few visible defects.

Reflectivity data for some samples were obtained with a Digilab FTS60 Fourier transform spectrometer interfaced to a Barnes Spectratech Universal Infrared Microsampling Accessory. This microscope attachment allows the study of microscopic samples or of small areas of larger samples. On-axis optics function as a binocular microscope with 320X viewing power, allowing visual observation of the sample prior to data collection. A double-slit configuration allows continuously variable sampling size, and condensing optics direct the reflected beam to the dewar of an optimized 77 K detector. The range of 4400–700 cm^{-1} utilizes a conductive ceramic source, a HgCdTe (MCT) cell as a detector, and a Ge film on KBr beam splitter. A quartz beam splitter, a tungsten halogen bulb, and an InSb detector cover the near-infrared region (12 500–3300 cm^{-1}). The substantial overlay of the regions on this instrument ensures good continuity between ranges. A high quality front surface gold mirror is used for calibration.

Other reflectance spectra were acquired with a Perkin-Elmer Model 180 dual-range infrared spectrometer (from 4000 to 50 cm^{-1}) and with a Zeiss MM12 double monochromator incorporating interchangeable glass and quartz prisms (from 50 000 to 4000 cm^{-1}). The BCD output of the Zeiss lock-in amplifier is interfaced to an IBM PC via a Keithley Series 500 Measurement Control System. This instrumentation is described in detail elsewhere.[8,10] Reflectivity data from the different instruments agreed to within ±1%. All optical data were analyzed with a FORTRAN program, described in detail elsewhere,[11] and implemented on a Control Data Cyber 845 mainframe computer.

Charge-Transport Measurements. DC electrical conductivity and thermopower measurements were made on polycrystalline compactions of $\{[Si(Pc)O]X_y\}_n$ in pellet form similar to those used for diffraction[2] and optical reflectance studies (vide supra). Conductivity measurements were performed in the usual four-probe geometry with 60- and 25-μm gold wires used for the current and voltage electrodes, respectively. Measurements of the pellet cross-sectional area and voltage probe separation were made with a calibrated binocular microscope. Conductivity data were obtained with the computer-automated system described elsewhere.[12] Thermoelectric power measurements were made by using a slow ac technique[13] with 60-μm gold wires serving to support and conduct heat to the sample, as well as to measure the voltage across the sample resulting from the applied temperature gradient. In both measurements, the gold electrodes were held in place on the sample with a conductive gold paste.

Conductivity specimens were mounted on interchangeable sample holders, and thermopower specimens were mounted on a fixed sample holder/differential heater. Mounted samples were placed under vacuum (10^{-3} Torr) and heated to 320 K for 2–4 h to cure the gold contacts. For a variable-temperature run, data (conductivity or thermopower) were acquired during both sample cooling and warming to check reversibility. The temperature drift rate during an experiment was kept below 1 K/min. Typically, three to four separate variable-temperature runs were carried out for each sample stoichiometry to ensure reproducibility and stability. At a given temperature, reproducibility was within ±5%.

Thermoelectric power results collected by the slow-ac technique require the production of a slowly varying periodic temperature gradient across the samples and measuring the resulting sample voltage. Samples were suspended between the quartz block heaters by 60-μm gold wires thermally grounded to the blocks with GE 7031 varnish. The thermopower of a sample is given by eq 1, where the correction for the thermoelectric power of gold is calculated from a polynomial fit to the data of Huebener.[14] The magnitude of the applied temperature gradient was generally 3–4 K. Smaller temperature gradients gave essentially the same results but with somewhat lower sensitivity. Comparisons with temperature-dependent thermopower measurements on standard samples of lead,[15] manganin,[16] and $TEA(TCNQ)_2$[17] indicate results with this apparatus to be accurate to better than ±5% above 40 K and to better than ±10% between 4.2 and 40 K, where the increased uncertainty is partly due to the large phonon drag peak of gold. The exact location and magnitude of this peak is known to be dependent on impurity levels, manufacturing methods, etc. for the gold wire.[18]

$$S_{sample} = (\text{slope of voltage - temperature data})(S_{thermocouple}) + S_{gold} \quad (1)$$

Results

The synthesis and chemical and structural properties of the $\{[Si(Pc)O](BF_4)_y\}_n$, $\{[Si(Pc)O](TOS)_y\}_n$, and $\{[Si(Pc)O](SO_4)_y\}_n$ materials are described in the accompanying contribution.[2] The present account focuses first upon the conductivity and the thermoelectric power characteristics of these partially oxidized

(6) Preliminary accounts: (a) Almeida, M.; Gaudiello, J. G.; Marks, T. J.; Butler, J. C.; Marcy, H. O.; Kannewurf, C. R. *Synth. Met.* **1987**, *21*, 261–266. (b) Gaudiello, J. G.; Almeida, M.; Marks, T. J.; McCarthy, W. J.; Butler, J. C.; Kannewurf, C. R. *J. Phys. Chem.* **1986**, *90*, 4917–4920.

(7) (a) Hoffmann, R. *Angew. Chem., Int. Ed. Engl.* **1987**, *26*, 846–878, and references therein. (b) Whangbo, M.-H. In *Crystal Chemistry and Properties of Materials with Quasi-One-Dimensional Structures*; Rouxel, J., Ed.; D. Reidel: Dordrecht, The Netherlands, 1986; pp 27–85, and references therein.

(8) (a) Inabe, T.; Gaudiello, J. G.; Moguel, M. K.; Lyding, J. W.; Burton, R. L.; McCarthy, W. J.; Kannewurf, C. R.; Marks, T. J. *J. Am. Chem. Soc.* **1986**, *108*, 7595–7608. (b) Diel, B. N.; Inabe, T.; Lyding, J. W.; Schoch, K. F., Jr.; Kannewurf, C. R.; Marks, T. J. *J. Am. Chem. Soc.* **1983**, *105*, 1551–1567.

(9) (a) Earnshaw, A. *Introduction to Magnetochemistry*; Academic Press: London, 1968. (b) O'Connor, C. J. *Prog. Inorg. Chem.* **1982**, *29*, 203–283.

(10) Rau, J. W.; Kannewurf, C. R. *Zeiss-Mitt. Fortschr. Tech. Opt.* 1970, *5*, 199–209.

(11) (a) McCarthy, W. J. MS Thesis, Northwestern University, 1986. (b) McCarthy, W. J.; Kannewurf, C. R.; Inabe, T.; Marks, T. J.; Burton, R. L. In *Basic Properties of Optical Materials*, NBS Special Publication 697; National Bureau of Standards: Washington, DC, 1985; pp 54–57.

(12) Lyding, J. W.; Marcy, H. O.; Marks, T. J.; Kannewurf, C. R. *IEEE Trans. Instrum. Meas.* **1988**, *37*, 76–80.

(13) Chaikin, P. M.; Kwak, J. F. *Rev. Sci. Instrum.* **1975**, *46*, 218–220.

(14) Huebener, R. P. *Phys. Rev.* **1964**, *136*, A1740–A1744.

(15) Christian, J. W.; Jan, J. P.; Pearson, W. B.; Templton, I. B. *Proc. R. Soc. A* **1958**, 213–221.

(16) Rathnayaka, K. D. D. *J. Phys. E* **1985**, *18*, 380–381.

(17) Farges, J. P.; Brau, A. *Phys. Status Solidi B* **1974**, *64*, 269–275.

(18) (a) Andersen, H. H.; Nielsen, M. *Phys. Lett.* **1963**, *6*, 17–18. (b) Polāk, J. *Czech. J. Phys. B* **1963**, *13*, 616–618. (c) Kopp, J. *Solid State Commun.* **1974**, *14*, 1059–1060.

Table I. Room-Temperature (300 K) Four-Probe Electrical Conductivity Data for Polycrystalline $\{[Si(Pc)O]X_y\}_n$ Polymers

y	σ(300 K), Ω^{-1} cm^{-1}	y	σ(300 K), Ω^{-1} cm^{-1}
	$\{[Si(Pc)O](BF_4)_y\}_n$		
0.00[a]	3.0×10^{-8}	0.27	$2.9\ (7) \times 10^{-2}$
0.00[b]	2.2×10^{-6}	0.36	$1.8\ (4) \times 10^{-1}$
0.13	$3.3\ (15) \times 10^{-3}$	0.41	$1.2\ (3) \times 10^{-1}$
0.19	$1.4\ (3) \times 10^{-2}$	0.50	$1.3\ (3) \times 10^{-1}$
	$\{[Si(Pc)O](TOS)_y\}_n$		
0.10	$5.6\ (2) \times 10^{-4}$	0.37	$3.7\ (8) \times 10^{-2}$
0.19	$1.0\ (6) \times 10^{-2}$	0.52	$4.5\ (10) \times 10^{-2}$
0.28	$2.0\ (9) \times 10^{-2}$	0.67	$4.3\ (11) \times 10^{-2}$
	$\{[Si(Pc)O](SO_4)_y\}_n$		
0.040	$8.5\ (4) \times 10^{-3}$	0.095	$8.8\ (3) \times 10^{-2}$

[a] Orthorhombic. [b] Tetragonal.

polymers as a function of counterion and y. Next, the optical properties are discussed with a view toward probing electronic structure as a function of counterion and y. The magnetic properties are also examined by static susceptibility and electron spin resonance (ESR) techniques as a function of both counterion and y. Finally, the Discussion concentrates on interpretation and how the present results compare with other molecular metals and conductive polymers.

Charge Transport. Four-Probe Electrical Conductivity. Direct current four-probe electrical conductivity measurements were performed on the same type of compressed polycrystalline sample pellets as were employed for the X-ray diffraction[2] and optical reflectance (vide infra) studies. Techniques and precautions were the same as those described previously.[8] It is expected that conductivity results on polycrystalline samples of low-dimensional conductors will be influenced by the isotropy of the measurement technique and the effects of interparticle contact resistance. While measurements on high-quality single crystals would obviously be more desirable (although not exempt from their own ambiguities and artifacts[19]), such sample types are not currently available for any type of doped conductive polymer, and polycrystalline conductivity data can still be highly informative.[8] This should be especially true for a chemically related series of materials having the same chemical precursor and similar chemical compositions and crystal structures, and in which crystallite orientation information is in hand. A great deal of empirical results now indicate that the dc conductivities of low-dimensional molecular "metals" are typically 10^2–10^3 greater when measured on single-crystal specimens along the molecular stacking direction than when measured on compressed polycrystalline samples.[5d,8,20,21] The temperature dependence of the conductivity is also different for single crystals and polycrystalline compactions; however, the nature of the difference is qualitatively predictable,[8] and techniques exist (e.g., voltage-shorted compaction,[8b,22] thermoelectric power—vide infra) that reveal key aspects of single-crystal behavior even in polycrystalline samples. In regard to phthalocyanine materials, we have found the above single-crystal–polycrystalline generalizations to hold well for $Ni(Pc)(I_3)_{0.33}$,[8b] $H_2(Pc)(I_3)_{0.33}$,[5e,20] and $Ni(Pc)(BF_4)_{0.33}$.[5c,20] It should therefore be possible to make reasonable extrapolations from polycrystalline $\{[Si(Pc)O]X_y\}_n$ conductivity data to anisotropic charge-transport behavior in the polymer chain direction.

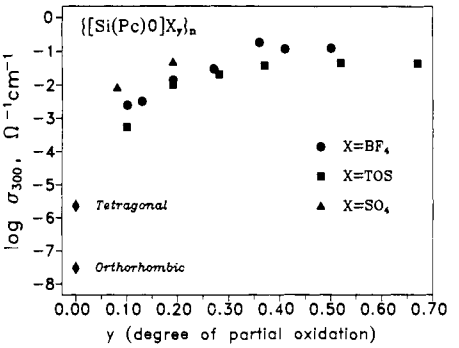

Figure 1. Electrical conductivity at 300 K for polycrystalline $\{[Si(Pc)O]X_y\}_n$ samples as a function of the degree of oxidation per Si(Pc) unit (y). The y values for $\{[Si(Pc)O](SO_4)_y\}_n$ have been multiplied by 2.0 to correct for the dinegative charge of SO_4^{2-}.

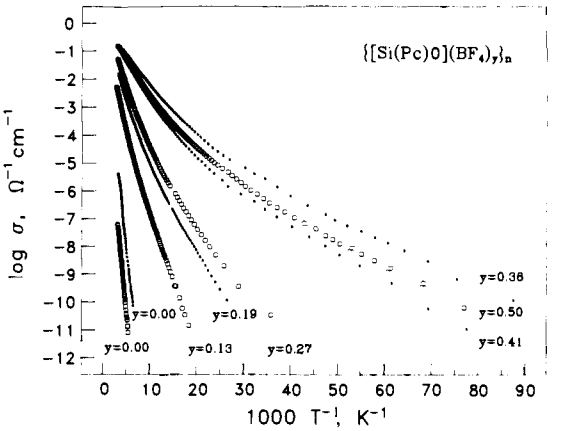

Figure 2. Variable-temperature electrical conductivity data for polycrystalline $\{[Si(Pc)O](BF_4)_y\}_n$ samples at various doping levels. The y = 0.00 data refer to the orthorhombic (○) and tetragonal (●) $[Si(Pc)O]_n$ phases.

Room temperature four-probe conductivity data for compressed polycrystalline samples of various $\{[Si(Pc)O]X_y\}_n$ materials are set out in Table I. That these results are not influenced by preferential crystallite orientation was demonstrated by using previously implemented techniques.[8] Room temperature data as a function of doping stoichiometry are plotted in Figure 1 for $X^- = BF_4^-$ and TOS^-. The general behavior is similar to that observed in numerous other conductive polymers[23] including chemically doped $\{[Si(Pc)O]X_y\}_n$ materials.[8] Upon incremental doping, an initial steep rise in conductivity is followed by a leveling off. The magnitudes in conductivity observed at a given doping level are roughly comparable for the electrochemically and chemically doped $\{[Si(Pc)O]X_y\}_n$ polymers, with the principal difference being the larger y values accessible for the electrochemically doped polymers. Hence, the flat region of such σ vs y curves now extends

(19) (a) Single-crystal conductivity measurements can be severely influenced by disorder, defects, impurities, and other factors related to the purity of the starting materials and the crystallization methodology.[5d,19b-e] In addition, even in cases of ideal contact alignment,[19f] other measurement-dependent phenomena such as contact strain[19g] and cooling rate effects[19g,h] can have major effects on the observed $\sigma(T)$. (b) Khanna, S. K.; Fuller, W. W.; Grüner, G.; Chaikin, P. M. *Phys. Rev. B.* **1981**, *24*, 2958–2963, and references therein. (c) Heeger, A. J. In *Highly Conducting One-Dimensional Solids*; Devreese, J. T., Evrard, R. P., van Doren, V. E., Eds.; Plenum Press: New York, 1979; pp 105–120. (d) Begg, I. D.; Roberts, K. J.; Sherwood, J. N.; Groth-Andersen, L.; Jacobsen, C. S. *Chem. Phys. Lett.* **1981**, *79*, 513–516. (e) Parkin, S. S.; Creuzet, F.; Jérome, D.; Fabre, J. M.; Bechgaard, K. *J. Phys. (Les Ulis, Fr.)* **1983**, *44*, 975–984. (f) Schafer, D. E.; Wudl, F.; Thomas, G. A.; Ferraris, J. P.; Cowan, D. O. *Solid State Commun.* **1974**, *14*, 347–351. (g) Inabe, T.; Lyding, J. W.; Kannewurf, C. R.; Marks, T. J., unpublished results. (h) Kagoshima, S.; Yasunaga, T.; Ishiguro, T.; Anzai, H.; Saito, G. *Solid State Commun.* **1983**, *46*, 867–870, and references therein.

(20) Almeida, M.; Butler, J. C.; Marcy, H. O.; Kannewurf, C. R.; Marks, T. J., manuscript in preparation.

(21) (a) Chiang, C. K.; Druy, M. A.; Gau, S. C.; Heeger, A. J.; Louis, E. J.; MacDiarmid, A. G.; Park, Y. W.; Shirakawa, H. *J. Am. Chem. Soc.* **1978**, *100*, 1013–1015. (b) Chiang, C. K.; Park, Y. W.; Heeger, A. J.; Shirakawa, H.; Louis, E. J.; MacDiarmid, A. G. *J. Chem. Phys.* **1978**, *69*, 5098–5104. (c) Farges, J. P.; Brau, A.; Gutmann, F. *J. Phys. Chem. Solids* **1972**, *33*, 1723–1726.

(22) Coleman, L. B. *Rev. Sci. Instrum.* **1978**, *49*, 58–62. This particular technique is at best of only qualitative value.

(23) (a) Roth, S.; Bleier, H. *Adv. Phys.* **1987**, *36*, 385–462. (b) Skotheim, T. A., Ed. *Handbook of Conducting Polymers*; Marcel Dekker: New York, 1986; Vol. 1, 2. (c) Frommer, J. E.; Chance, R. R. In *Encyclopedia of Polymer Science and Engineering*; Wiley: New York, 1986; Vol. 5, pp 471–493. (d) Wynne, K. J.; Street, G. B. *Ind. Eng. Chem. Prod. Res. Dev.* **1982**, *21*, 23–28. (e) Baughman, R. H.; Brēdas, J. L.; Chance, R. R.; Elsenbaumer, R. L.; Shacklette, L. W. *Chem. Rev.* **1982**, *82*, 209–222. (f) Wegner, G. *Angew. Chem., Int. Ed. Engl.* **1981**, *20*, 361–381.

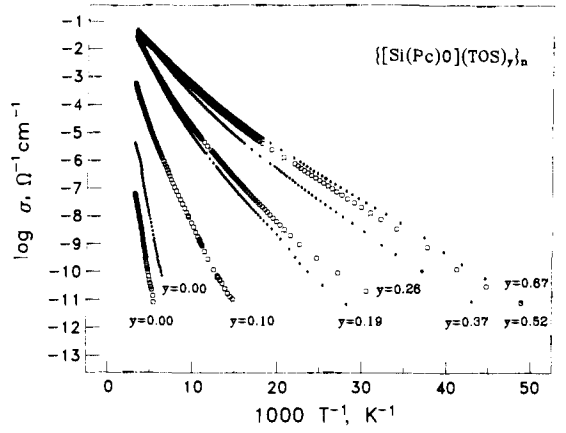

Figure 3. Variable-temperature electrical conductivity data for polycrystalline {[Si(Pc)O](TOS)$_y$}$_n$ samples at various doping levels. The y = 0.00 data refer to the orthorhombic (○) and tetragonal (●) [Si(Pc)O]$_n$ phases.

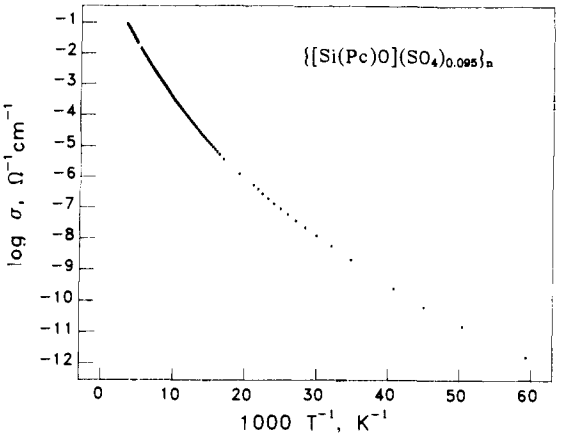

Figure 4. Variable-temperature electrical conductivity data for a polycrystalline sample of {[Si(Pc)O](SO$_4$)$_{0.095}$}$_n$.

over a fairly large range of band filling. It should be noted that the *chemical* doping of orthorhombic [Si(Pc)O]$_n$ was found to be inhomogeneous, i.e., for $y \lesssim 0.36$, {[Si(Pc)O]X$_y$}$_n$ is largely a mixture of doped and undoped phases.[8] In this case, the $\sigma(y)$ data could be fit to a three-dimensional percolation model for a randomly dispersed mixture of conductive and nonconductive particles.[8,24] That the electrochemically (homogeneously) doped polymers appear to adhere to a similar $\sigma(y)$ relationship is not a priori expected and will be taken up in the Discussion. Although the {[Si(Pc)O](SO$_4$)$_y$}$_n$ series was not investigated as extensively, Table I and Figure 1 show that the conductivity at the maximum doping level achieved ($y \approx 0.095$; $\rho \approx +0.19$) is not exceptional. In particular, there is no evidence that the dinegative counterion impedes charge transport. By use of the aforementioned empirical single crystal → compressed powder conversion factor, it is estimated that maximum conductivities in the phthalocyanine stacking direction will be ca. 20–100 Ω^{-1} cm^{-1} for the electrochemically doped {[Si(Pc)O]X$_y$}$_n$ polymers.

Variable-temperature conductivity data for the present materials are given in a log σ vs $1/T$ format in Figures 2–4. The behavior is reminiscent of the chemically doped {[Si(Pc)O]X$_y$}$_n$ materials[8] with generally falling apparent activation energies (slopes)/increasingly metallic character at progressively higher doping levels and decreasing slopes at lowest temperatures. In the case of the chemically (inhomogeneously) doped polymers, the $\sigma(T)$ data[8]

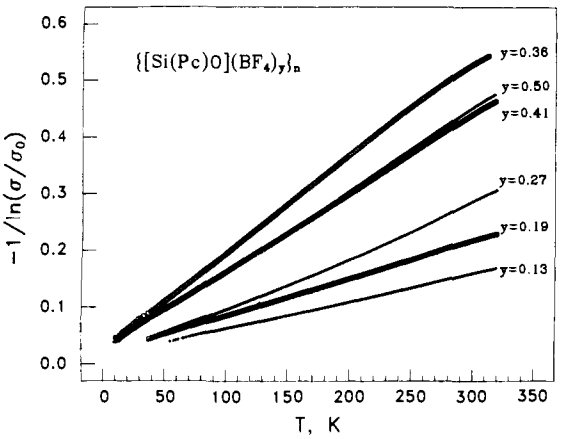

Figure 5. Conductivity data for polycrystalline {[Si(Pc)O](BF$_4$)$_y$}$_n$ samples plotted according to the fluctuation-induced carrier tunneling model of eq 2.

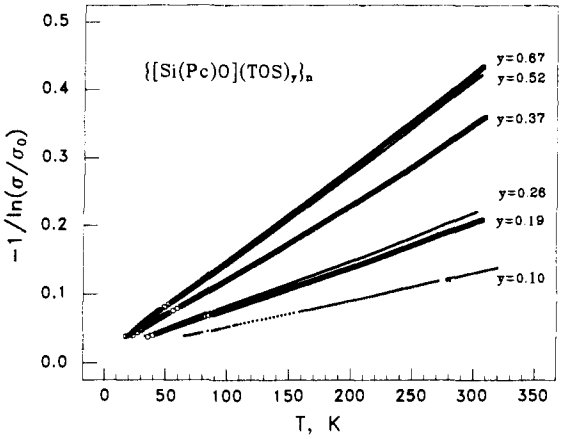

Figure 6. Conductivity data for polycrystalline {[Si(Pc)O](TOS)$_y$}$_n$ samples plotted according to the fluctuation-induced carrier tunneling model of eq 2.

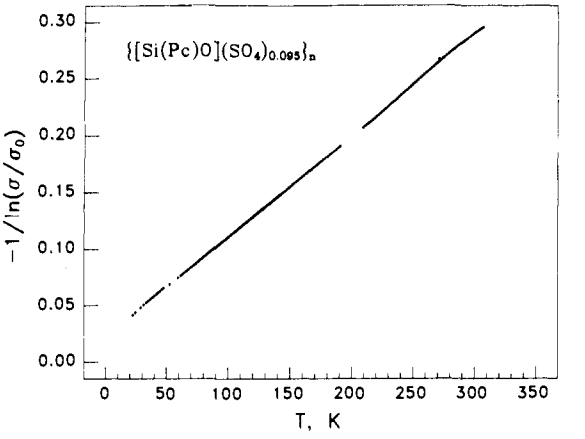

Figure 7. Conductivity data for a polycrystalline {[Si(Pc)O](SO$_4$)$_{0.095}$}$_n$ sample plotted in accordance with the fluctuation-induced tunneling model of eq 2.

can best be fit for all y to a fluctuation-induced carrier tunneling model originally developed for composites.[25] Here transport involves relatively large conductive regions separated by insulating barriers having a parabolic potential. Transport is thermally activated at higher temperatures but occurs predominantly via

(24) (a) Lundberg, B.; Sundqvist, B. *J. Appl. Phys.* **1986**, *60*, 1074–1079, and references therein. (b) Hsu, W. Y.; Barkley, J. R.; Meakin, P. *Macromolecules* **1980**, *13*, 198–200. (c) Lagues, M.; Sauterey, C. *J. Phys. Chem.* **1980**, 84, 3503–3508. (d) Clarke, P. S.; Orton, J. W.; Guest, A. J. *Phys. Rev. B* **1978**, *18*, 1813–1817. (e) Seager, C. H.; Pike, G. E. *Phys. Rev. B* **1974**, *10*, 1435–1446. (f) Kirkpatrick, S. *Rev. Mod. Phys.* **1973**, *45*, 574–588.

(25) (a) Sheng, P. *Phys. Rev. B* **1980**, *21*, 2180–2195. This model was originally derived for a three-dimensional system. In the present case, it is being applied to a quasi-one-dimensional system with significant two- or three-dimensional character. (b) Park, Y.-W.; Heeger, A. J.; Druy, M. A.; MacDiarmid, A. G. *J. Chem. Phys.* **1980**, *73*, 946–957.

Table II. Fluctuation-Induced Tunneling Analysis Parameters for Polycrystalline $\{[Si(Pc)O]X_y\}_n$ Materials

	fit param[a]		tunnel junction param[b]			
y	T_0	T_1	W^{m_0}, Å	$V_0^{m_0}$, eV	W^{m*}, Å	V_0^{m*}, eV
			$\{[Si(Pc)O](BF_4)_y\}_n$			
0.27	35.8	1541	194	8.0×10^{-2}	104	6.0×10^{-2}
0.36	17.3	613	196	5.1×10^{-2}	105	3.8×10^{-2}
0.41	19.8	756	194	5.6×10^{-2}	104	4.2×10^{-2}
0.50	20.4	750	194	5.6×10^{-2}	104	4.1×10^{-2}
			$\{[Si(Pc)O](TOS)_y\}_n$			
0.28	22.3	1276	250	8.3×10^{-2}	182	7.1×10^{-2}
0.37	15.2	936	282	7.5×10^{-2}	189	6.2×10^{-2}
0.52	10.3	750	337	7.4×10^{-2}	212	5.9×10^{-2}
0.67	13.4	775	279	6.8×10^{-2}	169	5.3×10^{-2}
			$\{[Si(Pc)O](SO_4)_y\}_n$			
0.095	22.2	1080	224	7.3×10^{-2}	2.15	7.1×10^{-2}

[a] Parameters derived from least-squares fit to eq 2. [b] Parameters calculated from above fit, making certain assumptions about carrier masses (m_0 is the free electron mass; m^* is derived from the optical analysis) and junction cross-sectional area (see text).

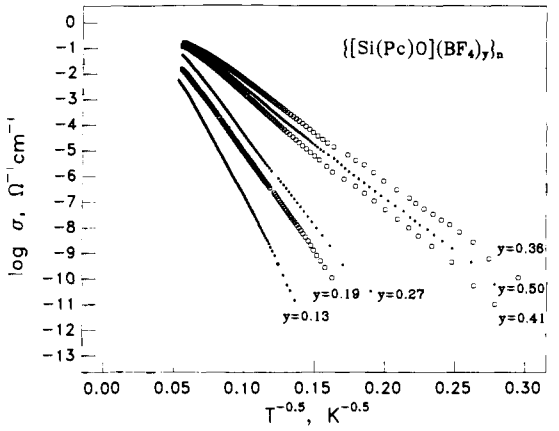

Figure 8. Attempted fit of $\{[Si(Pc)O](BF_4)_y\}_n$ variable-temperature conductivity data to the hopping model of eq 5 where $a = 0.50$.

elastic tunneling at low temperatures. Such behavior is described by eq 2–4 where A is the barrier cross-sectional area (in Å^2), V_0

$$\sigma = \sigma_0 e^{-|T_1/(T+T_0)|} \quad (2)$$

$$T_1 = 2AV_0^2/\pi e^2 kW \quad (3)$$

$$T_0 = 4\hbar AV_0^{3/2}/\pi^2 e^2 kW^2(2m)^{1/2} \quad (4)$$

is the barrier height (in eV), k is Boltzmann's constant, W is the barrier thickness (in Å), and m is the effective mass of the carrier.

Attempts to fit $\sigma(T)$ data for the electrochemically doped $\{[Si(Pc)O]X_y\}_n$ materials to the fluctuation-induced tunneling transport model met with reasonable success. As can be seen in Figures 5–7, adherence to eq 2 is good for most stoichiometries (see expanded scale plots of low doping stoichiometries in the Supplementary Materials). Nevertheless, there is evidence that a fluctuation-induced tunneling model may not be suitable for low y values. First, tunnel junction parameters derived from the curve fitting (Table II) evidence anomalous T_1 values. To the extent that T_1 values can be thought of as energy gaps,[25] the present parameters for low y values are unprecedented and seem unrealistic for the lightly doped $\{[Si(Pc)O]X_y\}_n$ materials. Second, it will be seen that an alternative transport model (vide infra) is equally applicable to the lightly doped materials. Assuming the carrier masses obtained in the optical analyses (vide infra) and that A is on the order of Pc ring dimensions (ca. 200 Å^2), it is possible to roughly estimate barrier thicknesses and heights within the framework of this model (Table II).

Attempts were also made to fit the $\sigma(T)$ data to eq 5, where $a = 0.25$ corresponds to a model involving three-dimensional variable range hopping between localized states,[26-28] and $a = 0.50$

$$\sigma = Ae^{-(T_0/T)^a} \quad (5)$$

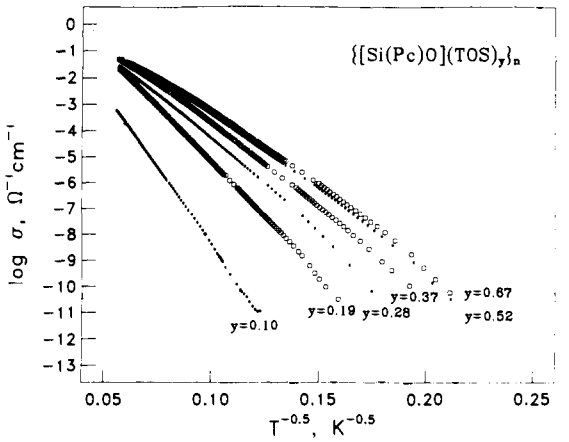

Figure 9. Attempted fit of $\{[Si(Pc)O](TOS)_y\}_n$ variable-temperature conductivity data to the hopping model of eq 5 where $a = 0.50$.

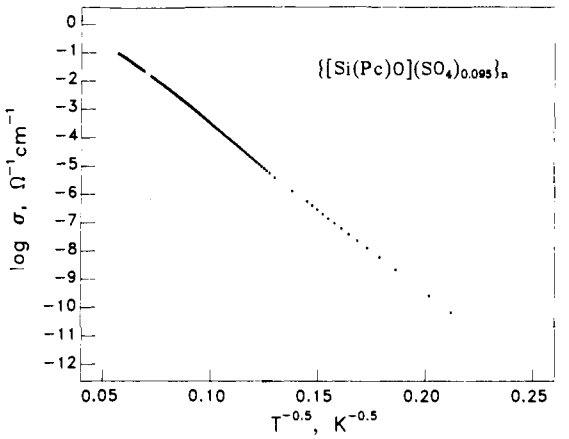

Figure 10. Attempted fit of $\{[Si(Pc)O](SO_4)_{0.095}\}_n$ variable-temperature conductivity data to the transport model of eq 5 where $a = 0.50$.

corresponds to models involving carrier tunneling between small metallic particles (e.g., granular metals) in a nonconductive matrix,[29] one-dimensional carrier hopping between localized states,[30] or transport in the presence of certain types of disorder.[30] As can be seen in Figures 8–10, the $\sigma(T)$ fit for $a = 0.50$ is visually at least as good for the lightly doped $\{[Si(Pc)O]X_y\}_n$ materials as is the fit to the fluctuation-induced tunneling model. Less convincing fits to the $a = 0.25$ model are shown as Supplementary Material. For doped polypyrrole and polythiophene, a variable range hopping model ($a = 0.25$) appears to best fit the $\sigma(T)$ data,[31] while a granular metal ($\alpha = 0.50$) description has been invoked for polyaniline.[32] The situation for heavily doped polyacetylene

(26) (a) Mott, N. F. *Festkoerperprobleme* **1979**, *19*, 333–361. (b) Mott, N. F.; Davis, E. A. *Electronic Processes in Non-Crystalline Materials, 2nd ed.*; Clarendon: Oxford, 1979; Chapters 1, 2.

(27) Epstein, A. J.; Rommelmann, H.; Bigelow, R.; Gibson, H. W.; Hoffman, D. M.; Tanner, D. B. *J. Phys.* **1983**, *C3*, 61–68.

(28) Colson, R.; Nagles, P. *J. Non-Cryst. Solids* **1980**, *36*, 129–134, and references therein.

(29) (a) Sheng, P.; Abeles, B.; Arie, Y. *Phys. Rev. Lett.* **1973**, *31*, 44–47. (b) Sichel, E. K.; Gittleman, J. I.; Sheng, P. *Phys. Rev. B* **1978**, *18*, 5712–5716. (c) Sichel, E. K. *Appl. Phys. Commun.* **1981**, *1*, 83–96. (d) Abeles, B.; Sheng, P.; Coutts, M. D.; Arie, Y. *Adv. Phys.* **1975**, *24*, 407–461.

(30) (a) Tomkiewicz, Y.; Shiren, N. S.; Schultz, T. D.; Thomann, H.; Dalton, L. R.; Zettl, A.; Grüner, G.; Clarke, T. C. *Mol. Cryst. Liq. Cryst.* **1982**, *83*, 17–31. (b) Mortensen, K.; Thewalt, M. L. W.; Tomkiewicz, Y.; Clarke, T. C.; Street, G. B. *Phys. Rev. Lett.* **1980**, *45*, 490–493.

(31) (a) Shen, Y.; Carneiro, K.; Jacobson, C.; Qian, R.; Qiu, J. *Synth. Met.* **1987**, *18*, 77–83, and references therein. (b) Bender, K.; Gogu, E.; Henning, I.; Schweitzer, D.; Müenstedt, H. *Synth. Met.* **1987**, *18*, 85–88, and references therein.

(32) (a) Zuo, F.; Angelopoulos, M.; MacDiarmid, A. G.; Epstein, A. J. *Phys. Rev. B.* **1987**, *36*, 3475–3478. (b) McCall, R. P.; Ginder, J. M.; Roe, M. G.; Asturias, G. E.; Scherr, E. M.; MacDiarmid, A. G.; Epstein, A. J. *Phys. Rev. B.* **1989**, *39*, 10174–10178.

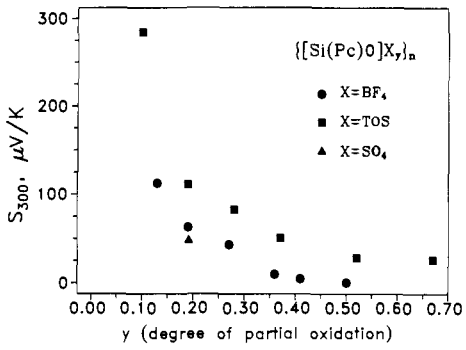

Figure 11. Room-temperature thermoelectric power data for {[Si(Pc)O](BF$_4$)$_y$}$_n$, {[Si(Pc)O](TOS)$_y$}$_n$, and {[Si(Pc)O](SO$_4$)$_{0.095}$}$_n$ conductive polymers.

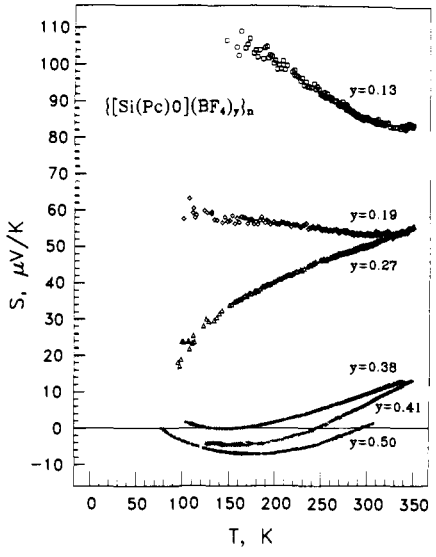

Figure 12. Variable-temperature thermoelectric power data for polycrystalline {[Si(Pc)O](BF$_4$)$_y$}$_n$ samples.

is not completely resolved.[23a] Thus, for the present {[Si(Pc)O]X$_y$}$_n$ polymers, the evidence for a possible divergence in transport mechanisms at low y between chemically (inhomogeneously) and electrochemically (homogeneously) doped materials is most interesting. The significance of the $y \approx 0.20$ stoichiometry/band filling to transport characteristics will be a topic of the Discussion.

Charge Transport. Thermoelectric Power. In contrast to electrical conductivity, thermoelectric power (TEP) measurements should be far less susceptible to artifacts introduced by the polycrystalline nature of samples and should more directly probe intrinsic transport properties.[25b,33] Thus, TEP is a zero-current technique and temperature drops at grain boundaries should be far less significant than voltage drops. As an illustration, single-crystal conductivity measurements on H$_2$(Pc)(I$_3$)$_{0.33}$ crystals in the macrocycle stacking direction reveal metallic conductivity ($\sigma \sim T^{-1.9}$) down to ca. 60 K, while compressed polycrystalline powders display far lower conductivities and thermally activated behavior below 270 K.[8b,5e] In contrast, variable-temperature single-crystal and compressed powder TEP data for H$_2$(Pc)(I$_3$)$_{0.33}$ are very similar in magnitude and temperature dependence and are indicative of a p-type metal ($S \sim T$),[33,34] with any differences in data attributable to grain boundary effects and/or minor deviations[5a] in sample stoichiometry.[35]

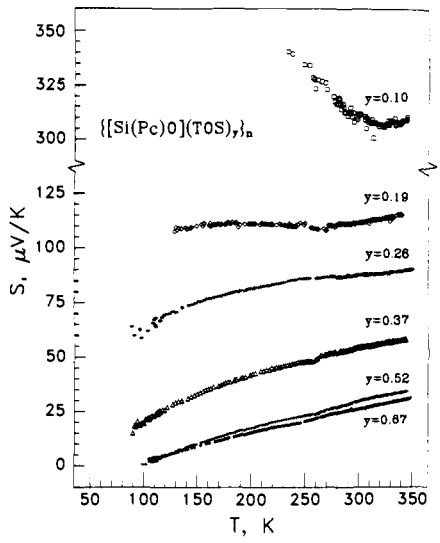

Figure 13. Variable-temperature thermoelectric power data for polycrystalline {[Si(Pc)O](TOS)$_y$}$_n$ samples.

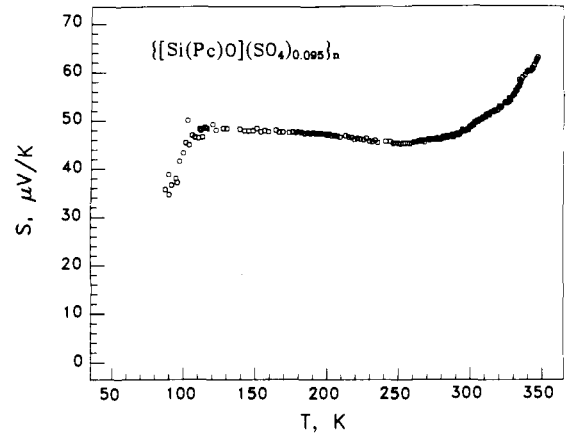

Figure 14. Variable-temperature thermoelectric power data for a polycrystalline sample of {[Si(Pc)O](SO$_4$)$_{0.095}$}$_n$.

Room temperature thermoelectric power data for the {[Si(Pc)O]X$_y$}$_n$ polymers are shown in Figure 11. It can be seen that the $S_{300}(y)$ response is similar for the BF_4^-- and TOS^--containing materials and that the behavior of {[Si(Pc)O](SO$_4$)$_{0.095}$}$_n$ is unexceptional. Variable-temperature thermoelectric power data for {[Si(Pc)O](BF$_4$)$_y$}$_n$, {[Si(Pc)O](TOS)$_y$}$_n$, and {[Si(Pc)O](SO$_4$)$_{0.095}$}$_n$ materials are shown in Figures 12–14, respectively. Accurate measurements at lower temperatures were hindered by the very large sample resistivities. In the BF_4^-- and TOS^--containing materials at low doping levels ($y \lesssim 0.19$), the magnitude and temperature dependence of the TEP is characteristic of a p-type (radical-cation) molecular semiconductor.[33,36] For {[Si(Pc)O](SO$_4$)$_{0.095}$}$_n$ ($\rho \approx +0.19$), $S(T)$ is similar to that for {[Si(Pc)O](BF$_4$)$_{0.19}$}$_n$, arguing again that the divalent counterion induces no perceptible changes in the band structure. In the doping range $y \approx 0.19$–0.27, a rather drastic change in transport characteristics occurs for both BF_4^-- and TOS^--containing polymers, and the TEP data evolve toward that typical of a p-type low-dimensional molecular metal.[33,36,37] As examples of this latter

(33) (a) Kwak, J. F.; Beni, G.; Chaikin, P. M. *Phys. Rev. B* **1976**, *13*, 641–646. (b) Cooper, J. R.; Alavi, B.; Zhou, L.-W.; Beyermann, W. P.; Grüner, G. *Phys. Rev. B* **1987**, *35*, 8794–8796.

(34) (a) Almeida, M.; Butler, J. C.; Marcy, H. O.; Kannewurf, C. R.; Marks, T. J., manuscript in preparation. (b) For another example of the generally favorable agreement between single-crystal and polycrystalline TEP data in low-dimensional materials, see: Shchegolev, I. *Phys. Status Solidi A*, **1972**, *12*, 9, Figure 25.

(35) For a polycrystalline sample, the observed Seebeck coefficient should be sensitive to properties both parallel and perpendicular to the stacking

$$S = \frac{x\sigma_{\parallel}S_{\parallel} + 2y\sigma_{\perp}S_{\perp}}{x\sigma_{\parallel} + 2y\alpha_{\perp}}$$

direction, where x and y are the cross-sectional areas of interparticle contact. While $\sigma_{\perp} \ll \sigma_{\parallel}$,[5e] little is known about the sign and magnitude of $S_{\perp}$.

(36) (a) Mortensen, K.; Conwell, E. M.; Fabre, J. M. *Phys. Rev. B* **1983**, *28*, 5856–5862, and references therein. (b) Conwell, E. M. *Phys. Rev. B* **1978**, *18*, 1818–1823.

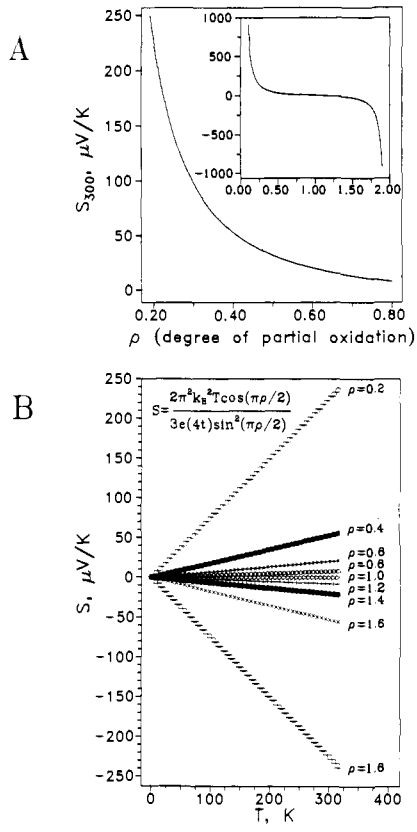

Figure 15. (A) Band filling dependence of thermoelectric power calculated for a simple tight-binding band structure with energy-independent scattering, negligible U, T = 300 K, and $4t$ = 0.60 eV (eq. 6). The inset shows the dependence for the full ρ = 0.00–2.00 range. (B) Temperature dependence of thermoelectric power as a function of degree of oxidation ρ for a simple tight-binding band structure with energy-independent scattering, negligible U, and $4t$ = 0.60 eV (eq 6).

type of behavior, room-temperature stacking axis single-crystal Seebeck coefficients (S_{300}) for $H_2(Pc)(I_3)_{0.33}$,[5b,e] $Ni(Pc)(I_3)_{0.33}$,[5c] $Ni(Pc)(BF_4)_{0.33}$,[5d] and $Ni(Pc)(ClO_4)_{0.42}$[5a] are ca. +60, +60, +50, and +25 μV/K, respectively. The temperature dependence of S in these molecular materials deviates significantly from the strict linearity predicted (but seldom observed[37]) by a simple tight-binding expression (eq 6, neglecting the energy dependence of the

$$S = \frac{2\pi^2 k_B^2 T \cos(\pi\rho/2)}{3e(4t)\sin^2(\pi\rho/2)} \quad (6)$$

scattering time and assuming small Coulomb correlations, U[38]) with varying degrees of decreasing slope at lower temperatures (prior to the onset of obvious metal → insulator transitions in $Ni(Pc)(I_3)_{0.33}$[5c] and $Ni(Pc)(BF_4)_{0.33}$[5d]). In eq 6, $4t$ is the bandwidth[3,39] while the other terms have their usual meaning.

For constant $4t$, eq 6 also predicts the dependence of $S(T)$ plots on ρ. This is shown in Figure 15 for $4t$ = 0.60 eV. It can be seen

(37) (a) Schweitzer, D.; Hennig, I.; Bender, K.; Endres, H.; Keller, H. J. *Mol. Cryst. Liq. Cryst.* **1985**, *120*, 213–220. (b) Mortensen, K.; Jacobsen, C. S.; Bechgaard, K.; Carneiro, K.; Williams, J. M. *Mol. Cryst. Liq. Cryst.* **1985**, *119*, 401–404. (c) Maaroufi, A.; Coulon, C.; Flandrois, S.; Delhaes, P.; Mortensen, K.; Bechgaard, K. *Solid State Commun.* **1983**, *48*, 555–559, and references therein. (d) Chaikin, P. M.; Grüner, G.; Shchegolev, I. F.; Yagubskii, E. B. *Solid State Commun.* **1979**, *32*, 1211–1214.

(38) (a) Ihle, D.; Eifrig, Th. *Phys. Status Solidi B* **1979**, *91*, 135–140. (b) Chaikin, P. M.; Beni, G. *Phys. Rev. B.* **1976**, *13*, 647–651.

(39) (a) Doris, K. A.; Ciliberto, E.; Fragalà, I.; Ratner, M. A.; Marks, T. J. In ref. 3d, pp 337–346. (b) Pietro, W. J.; Marks, T. J.; Ratner, M. A. *J. Am. Chem. Soc.* **1985**, *107*, 5387–5391. (c) Pietro, W. J.; Ellis, D. E.; Marks, T. J.; Ratner, M. A. *Mol. Cryst. Liq. Cryst.* **1984**, *10B*, 273–287. (d) Ciliberto, E.; Doris, K. A.; Pietro, W. J.; Reisner, G. M.; Ellis, D. E.; Fragalà, I.; Herbstein, F. H.; Ratner, M. A.; Marks, T. J. *J. Am. Chem. Soc.* **1984**, *106*, 7748–7761. (e) Hale, P. D.; Pietro, W. J.; Ratner, M. A.; Ellis, D. E.; Marks, T. J. *J. Am. Chem. Soc.* **1987**, *109*, 5943–5947.

Table III. Thermoelectric Power Data for $\{[Si(Pc)O]X_y\}_n$ Materials

y	$S(300)$, μV/K	$(\Delta S/\Delta T)_{\sim 300}$, μV/K²	$4t$, eV[a]
	$\{[Si(Pc)O](BF_4)_y\}_n$		
0.13	113 (22)		
0.19	62.9 (69)		
0.27	43.4 (67)	0.101 (27)	2.70 (72)
0.36	10.5 (35)	0.134 (44)	1.16 (41)
0.41	4.6 (30)	0.135 (13)	0.81 (8)
0.50	0.31 (32)	0.100 (11)	0.70 (7)
	$\{[Si(Pc)O](TOS)_y\}_n$		
0.10	284 (38)		
0.19	114 (12)		
0.28	82.1 (39)	0.079 (59)	4.2 (21)
0.37	50.9 (82)	0.115 (37)	1.27 (36)
0.52	28.2 (61)	0.109 (33)	0.63 (23)
0.67	26.0 (35)	0.096 (25)	0.36 (11)
	$\{[Si(Pc)O](SO_4)_y\}_n$		
0.095	48.6 (52)	0.17 (5)	3.8 (19)

[a] Tight-binding bandwidth derived from a fit to eq 6 near 300 K.

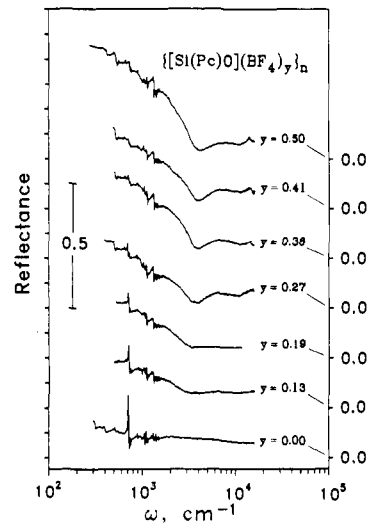

Figure 16. Optical reflectance spectra of compressed polycrystalline $\{[Si(Pc)O](BF_4)_y\}_n$ samples. Spectra are offset vertically by 0.2 reflectance unit for ease of viewing.

that the overall $S(y)$ behavior of the room-temperature TEP data adhere to the theoretical pattern (Figure 15A) reasonably well. For the heavily doped $\{[Si(Pc)O](BF_4)_y\}_n$ polymers with $y \gtrsim 0.36$, all materials exhibit rather similar $S(T)$ behavior with small, metallic magnitudes of S, a transition to slightly negative S values at lower temperatures, and pronounced curvature at lower temperatures. In contrast, the heavily doped $\{[Si(Pc)O](TOS)_y\}_n$ polymers ($y \gtrsim 0.28$) exhibit a somewhat greater dependence of S upon y, more linear $S(T)$, and less (if any) tendency to attain negative S values at lower temperatures. The $S(y)$ adherence to eq 6 over the full temperature range is perhaps slightly better for the $\{[Si(Pc)O](BF_4)_y\}_n$ polymers where some compression in $S(T)$ traces is observed at higher y (cf. Figure 15B). Thermoelectric power data are collected in Table III. Bandwidth parameters were obtained for the more metallike materials by linear least-squares fits to eq 6 in the relatively linear ($T > 250$ K) regions of the $S(T)$ data. For the heavily doped BF_4^- and TOS^- materials, reasonable agreement is observed with $4t$ derived from earlier reflectivity analyses of $\{[Si(Pc)O]X_y\}_n$ materials,[8] with reflectivity analyses of the present materials (vide infra), with PES-derived gas-phase $4t$ values,[39a,d] and with theoretical $4t$ values obtained via the DVM-Xα formalism.[39b-e] The reason why $4t$ values are unrealistically large at lower doping levels will be addressed in the Discussion.

Optical Reflectivity. Specular reflectance data on compressed polycrystalline samples can provide valuable information on electronic structure when appropriate adjustments are made for

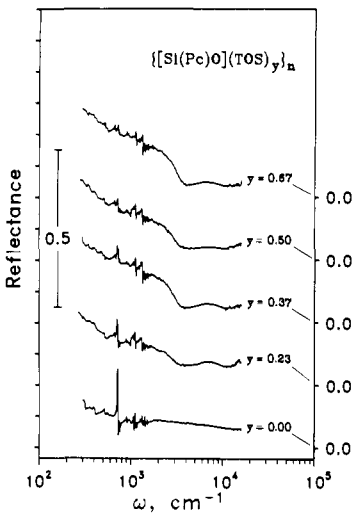

Figure 17. Optical reflectance spectra of compressed polycrystalline {[Si(Pc)O](TOS)$_y$}$_n$ samples. Spectra are offset vertically by 0.2 reflectance unit for ease of viewing.

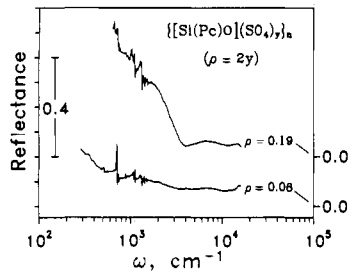

Figure 18. Optical reflectance spectra of compressed polycrystalline {[Si(Pc)O](SO$_4$)$_y$}$_n$ samples. Spectra are offset vertically by 0.20 reflectance unit for ease of viewing. $\rho = 2y$.

the polycrystalline nature of the specimens and any anisotropic crystallite orientation.[5a-f,8,11] When appropriate data analysis is applied, there is good agreement between results obtained from single-crystal and polycrystalline samples. Specular reflectance spectra for compressed polycrystalline {[Si(Pc)O](BF$_4$)$_y$}$_n$, {[Si(Pc)O](TOS)$_y$}$_n$, and {[Si(Pc)O](SO$_4$)$_y$}$_n$ samples are shown in Figures 16–18, respectively. Viewed as a function of y, the former two data sets both exhibit rather featureless (except for molecular features) spectra typical of semiconductors[40] at low doping levels. However, in the region $y \gtrsim 0.20$, the appearance of a plasma edge, typical of a low-dimensional molecular metal,[2,5a-e,8,40,41] is noted. As in the other physical measurements, the {[Si(Pc)O](SO$_4$)$_{0.095}$}$_n$ reflectance data give no evidence for localization of the band structure. As y is increased beyond 0.20–0.30, the {[Si(Pc)O](BF$_4$)$_y$}$_n$ and {[Si(Pc)O](TOS)$_y$}$_n$ data exhibit a shift of the plasma edge to higher energies, in accord with simple tight-binding band theoretical expectations (vide infra). In contrast, chemically (inhomogeneously) doped {[Si(Pc)O]X$_y$}$_n$ materials do not exhibit a detectable shift in the plasma edge with increasing y.[8] Rather, and in accord with the largely two-phase (undoped + doped) character of these latter materials, the edge becomes more pronounced (the reflectivity increases) but does not significantly shift in energy.

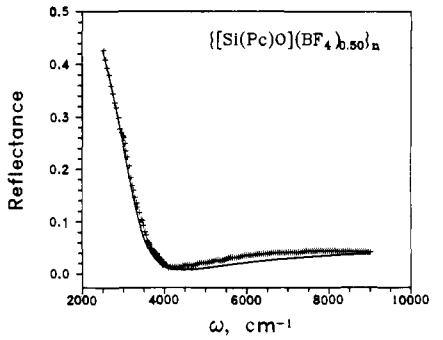

Figure 19. Optical reflectance spectrum of a polycrystalline {[Si(Pc)O](BF$_4$)$_{0.50}$}$_n$ sample (+ = experimental data points) and numerical fit to the data (solid line) yielding the parameters set out in Table IV.

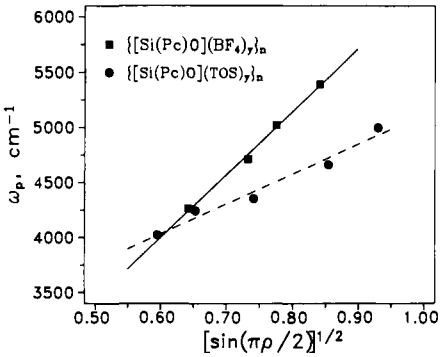

Figure 20. Plot of {[Si(Pc)O](BF$_4$)$_y$}$_n$ and {[Si(Pc)O](TOS)$_y$}$_n$ plasma frequencies (from reflectance data) as a function of degree of partial oxidation $\rho(y)$ according to eq 11.

After X-ray diffraction data were used to correct for preferential crystallite orientation,[8] the reflectance data[42] were fit to a Drude (electron gas) model for the dielectric function $\epsilon(\omega)$ (eq 7).[5a-e,8,40,41]

$$\epsilon(\omega) = \epsilon_{core} - \frac{\omega_p^2}{\omega^2 + i\omega/\tau} \tag{7}$$

Here ϵ_{core} is the dielectric constant at high frequency arising from the core polarizability, ω_p is the plasma frequency, and τ is the electronic relaxation time (for scattering near the Fermi surface). The plasma frequency can be related to the carrier density per unit volume, N_c, and the optical effective mass of the carriers, m^*, by eq 8. The majority carriers have been shown to be holes

$$\omega_p^2 = 4\pi N_c e^2/m^* \tag{8}$$

on the basis of the thermopower data (vide supra), and N_c can be calculated from the experimental degree of partial oxidation, ρ, and crystallographic data. An optically derived estimate of the low-frequency electrical conductivity can be obtained via eq 9.

$$\sigma_{opt} = \omega_p^2\tau/4\pi \tag{9}$$

For a simple one-dimensional tight-binding band structure, the plasma frequency can be related to the bandwidth (in the macrocycle stacking direction) and the Pc–Pc interplanar spacing, c, as shown in eq 10.[8,40,41] As already noted, previous condensed-

$$4t = \frac{\rho(\hbar\omega_p)^2}{4N_c e^2 c^2 \sin(\pi\rho/2)} \tag{10}$$

phase (reflectivity, TEP),[5a-e,8] gas-phase (PES),[39a,d] and theoretical (DVM-Xα)[39] estimations of $4t$ have been shown to be in good agreement for stacked phthalocyanine conductors.

Parameters derived from the present optical analyses on the metallike {[Si(Pc)O]X$_y$}$_n$ materials are set out in Table IV. An

(40) Jacobsen, C. S. In ref 3b, pp 253–274.

(41) (a) Madison, M. R.; Coleman, L. B.; Somoano, R. B. *Solid State Commun.* **1981**, *40*, 979–982. (b) Weinstein, B. A.; Slade, M. L.; Epstein, A. J.; Miller, J. S. *Solid State Commun.* **1981**, *37*, 643–646, and references therein. (c) Torrance, J. B.; Scott, B. A.; Welber, B.; Kaufman, F. B.; Seiden, P. E. Phys. *Rev. B.* **1979**, *19*, 730–741. (d) Delhaes, P.; Coulon, C.; Amiell, J.; Flandrois, S.; Toreilles, E.; Fabre, J. M.; Giral, L. *Mol. Cryst. Liq. Cryst.* **1979**, *50*, 43–58. (e) Jacobsen, C. S.; Mortensen, K.; Andersen, J. R.; Bechgaard, K. *Phys. Rev. B* **1978**, *18*, 905–921. (f) Somoano, R. B.; Yen, S. P. S.; Hadek, V.; Khanna, S. K.; Novotny, M.; Datta, T.; Hermann, A. M.; Woollam, J. A. *Phys. Rev. B* **1978**, *17*, 2853–2857.

(42)

$$R = \frac{1 + |\epsilon| - [2(\epsilon + \epsilon_1)]^{1/2}}{1 + |\epsilon| + [2(\epsilon + \epsilon_1)]^{1/2}}$$

where $\epsilon = (\epsilon_1^2 + \epsilon_2^2)^{1/2}$.

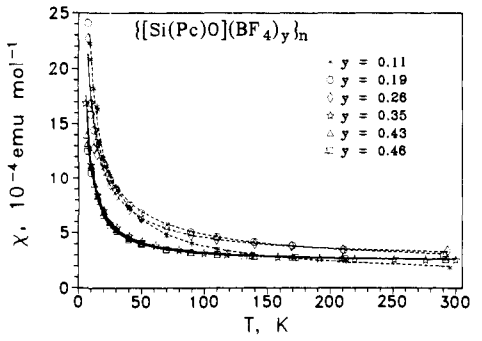

Figure 21. Variable-temperature static magnetic susceptibility of $\{[Si(Pc)O](BF_4)_y\}_n$ as a function of doping level. Lines through the data points represent the best fit to eq 12.

example of a typical numerical fit is shown in Figure 19. From Table IV, it can be seen that, for $y \gtrsim 0.25$, derived ω_p, ϵ_{core}, τ, $4t$, m/m_0, and σ_{opt} parameters for the present materials are in favorable agreement with previously derived values for other $\{[Si(Pc)O]X_y\}_n$ materials.[8] In particular, the σ_{opt} values are in reasonable agreement with the "rule-of-thumb" estimates from the powder conductivities (vide supra), and the bandwidth parameters are generally in the range [ca. 0.60 (6) eV] reported earlier.[8,39] The reason for the higher values of $4t$ observed at lower doping levels (near the boundary of metallike behavior) will be addressed in the Discussion. Slightly low values of $4t$ observed in several of the highly doped $\{[Si(Pc)O](TOS)_y\}_n$ materials, may arise from $\pi-\pi$ overlap-limiting structural distortions, which are not in discord with the diffraction data.[8] It can also be seen in Table IV that the plasma frequency data evidence an incremental shift to higher energies as y increases. Since $N_c = 2\rho$/unit cell volume, eq 10 reduces to eq 11, where B incorporates various

$$\omega_p = B\,[\sin(\pi\rho/2)]^{1/2} \qquad (11)$$

physical constants, the stacking distance, and the bandwidth. In Figure 20, it can be seen that the plasma frequency data for both BF_4^-- and TOS^--containing polymers fit eq 11 rather well. Clearly the major energetic displacements of $\omega_p(y)$ are explained satisfactorily within a tight-binding framework in terms of changes in the carrier density. Table IV and Figure 18 also reinforce the conclusions of the conductivity and TEP experiments that the divalent SO_4^{2-} counterion does not perturb the $[Si(Pc^{\rho+})O]_n$ band structure in any drastic way.

Static Magnetic Susceptibility and ESR. Static magnetic susceptibility studies of the electrochemically doped $\{[Si(Pc)O]X_y\}_n$ materials were carried out as a function of temperature using a highly sensitive SQUID susceptometer. Diamagnetic corrections and data analysis procedures are described in the Experimental Section. Detailed studies of susceptibility as a function of y were also carried out for the $\{[Si(Pc)O](BF_4)_y\}_n$ polymers. Representative data are shown in Figures 21 and 22. As found for other $\{[Si(Pc)O]X_y\}_n$ and $Ni(Pc)X_y/H_2(Pc)(I_3)_{0.33}$ materials,[5a-e,8] all of the present compounds exhibit "Curie tailing" at low temperatures. Such behavior ($\chi \sim T^{-\alpha}$, $\alpha \approx 0.8$–1.0) is a common magnetic characteristic of many polymeric and molecular conductors[3,4] and is usually ascribed to defects, impurities, or structural disorder.[3,43,44] For the present materials, the spin susceptibility data can be analyzed by decomposition into "Pauli-like" and "Curie-like" terms (eq 12), assuming in this case that the Curie

$$\chi_{total} = \chi_{Pauli} + AT^{-\alpha} \qquad (12)$$

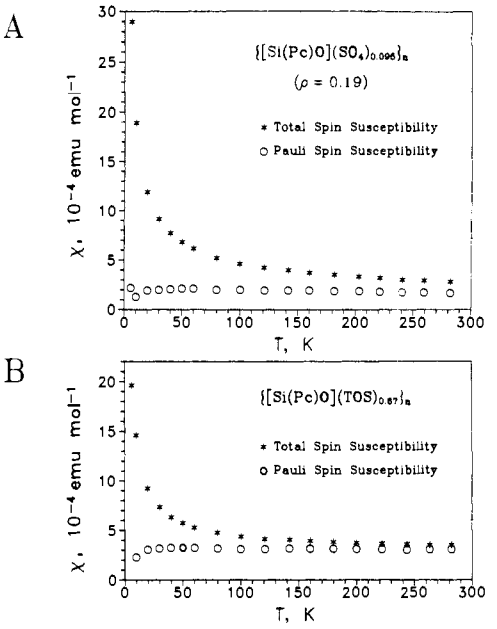

Figure 22. (A) Static magnetic susceptibility of $\{[Si(Pc)O](SO_4)_{0.095}\}_n$ as a function of temperature. Asterisks indicate total spin susceptibility and open circles the Pauli-like component. (B) Static magnetic susceptibility of $\{[Si(Pc)O](TOS)_{0.67}\}_n$ as a function of temperature. Asterisks indicate total spin susceptibility and open circles the Pauli-like component.

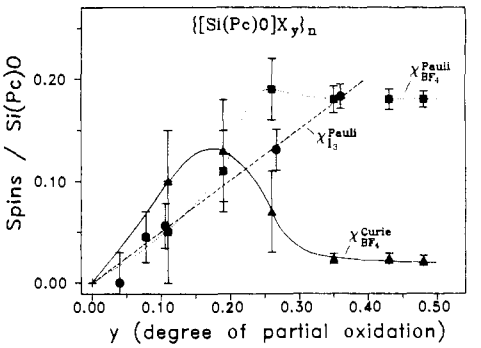

Figure 23. Stoichiometry dependence of the Pauli-like (■) and Curie-like (▲) spin susceptibilities of electrochemically (homogeneously) doped $\{[Si(Pc)O](BF_4)\}_n$ polymers. The dashed line indicates the stoichiometry dependence of the Pauli-like term (●) for chemically (inhomogeneously) doped materials (ref 8b).

component arises from isolated $S = {}^1/_2$, $g = 2.00$ sites. Data derived from this analysis are set out in Table V.

It can be seen that the susceptibilities of all electrochemically doped materials have a significant Pauli-like term. Similar observations have also been made for other phthalocyanine conductors,[5,8] and for comparable levels of y, the present χ_{Pauli} values are rather similar to those reported earlier.[5,8] The χ_P of $\{[Si(Pc)O](SO_4)_{0.095}\}_n$ provides no evidence for unusual localization effects (cf. the data for the other materials at $\rho \approx 0.19$), while the slightly higher χ_{Pauli} of $\{[Si(Pc)O](TOS)_{0.67}\}_n$ may reflect the high degree of partial oxidation or slight, structurally based band narrowing (cf. the reflectivity discussion). While the presence of substantial, weakly temperature-dependent Pauli-like contributions to the spin susceptibility is not universal for molecular conductors, it does have considerable precedent.[3,43,45] The present

(43) (a) Takahashi, M.; Sugano, T.; Kinoshita, M. *Bull. Chem. Soc. Jpn.* **1984**, *57*, 26–35. (b) Delhaes, P. Coulon, C.; Flandrois, S.; Hilti, B.; Mayer, C. W.; Rihs, G.; Rivory, J. *J. Chem. Phys.* **1980**, *73*, 1452–1463. (c) Isett, L. C. *Phys. Rev. B* **1978**, *18*, 439–447. (d) Scott, J. C.; Garito, A. F.; Heeger, A. J. *Phys. Rev. B* **1974**, *10*, 3131–3139.

(44) (a) Soos, Z. G.; Bondeson, S. R. *Mol. Cryst. Liq. Cryst.* **1982**, *85*, 19–31. (b) Tippie, L. C.; Clark, W. G. *Phys. Rev. B* **1981**, *23*, 5846–5853. (c) Azevedo, L. J.; Clark, W. G. *Phys. Rev. B* **1977**, *16*, 3252–3258. (d) Bulaevskii, L. N.; Zvarykina, A. V.; Karimov, Yu. S.; Lyubovskii, R. B.; Shchegolev, I. F. *Sov. Phys.-JETP (Engl. Transl.)* **1972**, *35*, 384–389.

(45) (a) Mazumdar, S.; Dixit, S. N. *Phys. Rev. B* **1986**, *34*, 3683–3699, and references therein. (b) Laversanne, R.; Amiell, J.; Coulon, C.; Garrigou-Lagrange, C.; Delhaes, P. *Mol. Cryst. Liq. Cryst.* **1985** *119*, 317–320. (c) Jacobsen, C. S.; Bechgaard, K. *Mol. Cryst. Liq. Cryst.* **1985** *120*, 71–78. (d) Coulon, C.; Delhaes, P.; Flandrois, S.; Lagnier, R.; Bonjour, E.; Fabre, J. M. *J. Phys. (Les Ulis, Fr.)* **1982**, *43*, 1059–1067. (e) It is possible that the finite character of the $[Si(Pc)O]_n$ chain lengths also introduces some temperature dependence in the magnetic susceptibility. The exact magnitude will depend on, among other factors, as yet unquantified aspects of interchain coupling.

Table IV. Optical Reflectance Data for $\{[Si(Pc)O]X_y\}_n$ Materials

y	tetrag lattice param, Å	charge trans ρ	plasma freq ω_p, cm^{-1}	backgrd dielec const ϵ_{core}	electr relaxn time τ, 10^{-15} s	bandwidth $4t$, eV	opt effect. mass ratio m/m_0	opt conductiv, Ω^{-1} cm^{-1}
				$\{[Si(Pc)O](BF_4)_y\}_n$				
0.27	a = 13.81 c = 6.65	0.27	4260	1.86	2.87	0.67 (6)	2.1	160
0.36	a = 13.85 c = 6.65	0.36	4710	2.37	5.10	0.64 (6)	2.1	355
0.41	a = 13.92 c = 6.65	0.41	5020	2.32	3.68	0.65 (6)	2.3	290
0.50	a = 13.97 c = 6.64	0.50	5390	2.58	4.96	0.63 (6)	2.4	450
				$\{[Si(Pc)O](TOS)_y\}_n$				
0.23	a = 13.95 c = 6.66	0.23	4020	2.06	3.07	0.71 (6)	2.0	160
0.28	a = 13.98 c = 6.65	0.28	4240	2.22	3.08	0.58 (6)	2.2	170
0.37	a = 14.09 c = 6.65	0.37	4350	2.04	3.52	0.55 (6)	2.7	210
0.52	a = 14.31 c = 6.64	0.52	4660	2.21	2.83	0.49 (6)	3.2	190
0.67	a = 14.39 c = 6.64	0.67	5000	2.32	3.51	0.48 (6)	3.5	275
				$\{[Si(Pc)O](SO_4)_y\}_n$				
0.095	a = 13.86 c = 6.67	0.19	4870	2.24	5.60	1.2 (1)	1.1	420

Table V. Static Magnetic Susceptibility Data for $\{[Si(Pc)O]X_y\}_n$ Materials[a]

y	χ_{Pauli}, 10^{-4} emu/mol	Pauli-like spins/M(Pc)[b]	fit param[a] A (10^{-4})	fit param[a] α	Curie-like spins/M(Pc)[c]	$4t$ magnetic, eV[d]	enhancement[e]
			$\{[Si(Pc)O](BF_4)_y\}_n$				
0.11[f]	0.68 (10)	0.05	135	0.82	0.10		
0.19[f]	1.40 (8)	0.11	16	0.67	0.13		
0.26[f]	2.39 (4)	0.19	101	0.83	0.07	0.43 (1)	1.6
0.35[g]	2.22 (6)	0.18	92	1.00	0.024	0.36 (1)	1.8
0.43[f]	2.28 (7)	0.18	90	1.00	0.024	0.29 (1)	2.2
0.50[f]	2.32 (6)	0.18	83	1.00	0.022	0.26 (1)	2.4
			$\{[Si(Pc)O](SO_4)_y\}_n$				
0.095[f] (ρ = 0.19)	1.93 (14)	0.15	116	0.82	0.09	0.35 (3)	3.4 (1.7[h])
			$\{[Si(Pc)O](TOS)_y\}_n$				
0.67[f]	3.13 (6)	0.25	124	1.00	0.032	0.56	0.9

[a] For $\chi = \chi_{Pauli} + AT^{-\alpha}$. [b] $N_p = {}^3\chi_{Pauli}kT/Ng^2\mu_B{}^2S(S+1)$, where T = 298 K. [c] $N_c = 3AT^{1-\alpha}k/Ng^2\mu_B{}^2S(S+1)$, where T = 298 K. [d] Bandwidth calculated from Pauli susceptibility by using eq 12. [e] $t_{optical}/t_{magnetic}$ at the same y value. [f] This work. [g] Chemically doped sample, from ref 8a. [h] Calculated with $4t$ = 0.60 eV.

χ_{Pauli} magnitudes appear to be typical of materials with comparable band fillings[3,43,45] and are considerably less than some exhibiting very large Coulomb enhancements.[45a]

Most interesting is the y dependence of the present $\{[Si(Pc)O](BF_4)_y\}_n$ susceptibilities (Figure 23) and how these differ from the y dependence for chemically (inhomogeneously) doped $\{[Si(Pc)O](BF_4)_y\}_n$ materials.[8b] In the latter system, Curie contributions are relatively insensitive to y (never exceeding 0.01–0.025 spins/macrocycle), and χ_P scales linearly with y (as indicated in Figure 23). Such behavior can be understood in terms of a two-phase system, with incremental doping creating increasing proportions of the fully doped, metallike (Pauli) phase.[8b] The Curie contribution can then be associated with impurities, defects, short chain lengths, etc. For the electrochemically (homogeneously) doped $\{[Si(Pc)O](BF_4)_y\}_n$ polymers, two rather different types of behavior are evident upon incremental doping (Figure 23): (i) χ_{Pauli} does not scale linearly with y, but rather climbs steeply from $y \approx 0.10$ to $y \approx 0.25$, and then remains nearly unchanged; (ii) χ_{Curie} rises steeply to a maximum of ca. 0.13 spins/Pc at $y \approx 0.20$, then falls precipitously, and remains at the low levels observed upon chemical doping.[8] Although it seems unrealistic to subject derived α values to extensive interpretation, it is noteworthy that for $y \lesssim 0.25$, α is consistently below 1.0 (suggestive of random exchange Heisenberg antiferromagnetic behavior or doping-induced random disorder[43a]) with the lowest value corresponding to the maximum χ_{Curie}. In the region where χ_{Curie} returns to more "normal" levels, α returns to ca. 1.0. These results complement both the charge-transport and optical data, which also suggest a major change in electronic structure at $y \approx 0.20$. That the Pauli-like susceptibilities of the $y \approx 0.36$ chemically, fully doped[8] and electrochemically doped materials are virtually identical (Figure 23) lends further credence to the overall chemical/electrochemical/structure/stoichiometry model.

Assuming a one-dimensional tight-binding band with noninteracting electrons (i.e., the Hubbard on-site Coulomb repulsion integral, U = 0) it is possible to relate the Pauli magnetic susceptibility to the intrastack transfer integral, t, as shown in eq 13.[46] Here N is Avogadro's number, μ_B is the Bohr magneton,

$$\chi_P = \frac{N\mu_B{}^2}{t\pi \sin(\pi\rho/2)} \tag{13}$$

and ρ is the degree of partial oxidation. Calculated "magnetic" bandwidths ($4t$) are compiled in Table V. Comparison with experimental $4t$ values obtained in the present study from optical (Table IV) or thermoelectric power (Table III) measurements or comparison to $4t$ data for other $\{[Si(Pc)O]X_y\}_n$ systems[8,39]

(46) (a) Shiba, H. *Phys. Rev. B* **1972**, *6*, 930–938. (b) Torrance, J. B.; Tomkiewicz, Y.; Silverman, B. D. *Phys. Rev. B* **1977**, *15*, 4738–4749.

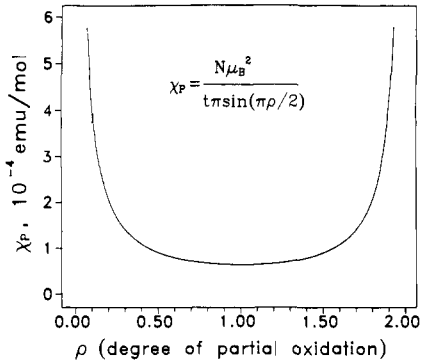

Figure 24. Band filling dependence of the Pauli magnetic susceptibility calculated according to the tight-binding description of eq 13 for $4t$ = 0.60 eV.

indicates, as discussed previously,[5a-e,8,39] that the magnetically derived band widths seriously underestimate $4t$. This phenomenon has been noted previously[3,36a,45,47,48] and has been attributed to enhancement of the magnetic susceptibility by on-site electron–electron Coulombic repulsion ($U \neq 0$) and/or by electron–phonon coupling. The present results provide the first experimental verification that this enhancement can indeed vary significantly[45a,47] in a single stacked system for wide excursions in ρ. In the case of $\{[Si(Pc)O](SO_4)_{0.095}\}_n$, the calculation of the enhancement incorporates a $4t$ based upon the optical reflectivity at the same ρ value (Table IV). It will be shown that such estimations are less accurate at low doping levels (vide infra). Use of $4t$ = 0.60 eV[39] yields a more normal enhancement factor of ca. 1.7 for the sulfate salt. Hence, there is no evidence that the off-axis dianion introduces any unusual screening effects in regard to on-site, electron–electron repulsions within the band structure (U). The data in Figure 23 also indicate that χ_{Pauli} falls slightly and then levels off in $\{[Si(Pc)O](BF_4)_y\}_n$ for y = 0.26 → 0.50. This plot is somewhat flatter but reproduces to some extent the flattening behavior predicted from eq 13 assuming, in this case, $4t$ = 0.60 eV (Figure 24). As for the thermopower and optical reflectivity (vide supra), deviations from behavior predicted by a simple tight-binding band model appear to be greatest at low doping levels. The reason will be taken up in the Discussion.

Electron spin resonance spectroscopy can provide valuable information on electronic structure and conduction electron spin dynamics. Data for the present materials are set out in Table VI. The line shapes are found to be relatively isotropic, and the magnitudes of the g values approach free electron values. As in the case of the chemically doped $\{[Si(Pc)O]X_y\}_n$ conductors,[8] this latter observation argues that the unpaired spin density resides in molecular orbitals that are primarily ligand (π radical cation) in character. Theoretical calculations and studies on $H_2(Pc)(I_3)_{0.33}$[5e] lead to the same conclusions.[29]

Figure 25 shows the room-temperature peak-to-peak ESR line widths for the $\{[Si(Pc)O](BF_4)_y\}_n$ and $\{[Si(Pc)O](TOS)_y\}_n$ materials over a wide range of oxidation states. The relatively broad line width at $y \approx 0.0$ is in accord with more localized spins.[49] Although the exact y dependence of line widths for the BF_4^- and TOS^- salts is slightly different, the general behavior of falling line width upon oxidative doping is in accord with the other physical measurements and with increasingly delocalized (mobile) conduction electrons and a relatively unidimensional band structure (the interstack transfer integral $t_\perp$ is small).[3,5a-e,50,51] In the case

Table VI. Powder ESR Data for $\{[Si(Pc)O]X_y\}_n$ Materials

y	g(300 K)	Γ(300 K),[a] G	Γ(77 K),[a] G
		$\{[Si(Pc)O](BF_4)_y\}_n$	
0.10	2.0022	0.35	
0.18	2.0022	0.55	0.80
0.26	2.0022	0.98	1.10
0.41	2.0021	0.65	
0.50	2.0024	0.95	1.05
		$\{[Si(Pc)O](TOS)_y\}_n$	
0.10	2.0033	0.87	
0.19	2.0025	0.75	
0.28	2.0024	0.65	0.68
0.37	2.0025	0.82	0.80
0.52	2.0024	0.98	
0.67	2.0023	0.55	0.55
		$\{[Si(Pc)O](SO_4)_y\}_n$	
0.040	2.0021	1.52	
0.095	2.0025	2.28	
		$[Si(Pc)O]_n$[b]	
0.00	2.0030	1.60	

[a] Observed linewidth. [b] Tetragonal phase.

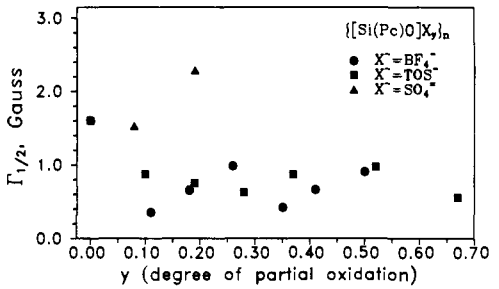

Figure 25. Room temperature peak-to-peak ESR line widths for powder $\{[Si(Pc)O](BF_4)_y\}_n$, $\{[Si(Pc)O](TOS)_y\}_n$, and $\{[Si(Pc)O](SO_4)_y\}_n$ samples as a function of y. The y values for the sulfate salt have been multiplied by 2.0 to correct for the dinegative charge.

of $X^- = TOS^-$, the $y = 0 \rightarrow 0.28$ line-width changes are relatively smooth, and any discontinuity accompanying an insulator-to-metal transition would then be associated with the small rise observed in the $y \gtrsim 0.30$ region. In contrast, the $\{[Si(Pc)O](BF_4)_y\}_n$ line-width data evidence a more abrupt discontinuity in the $y \approx$ 0.10–0.30 region. This latter response is somewhat reminiscent of that observed for reductive electrochemical doping of *trans*-polyacetylene ($(Na^+_y(CH)_y^-)_x$).[52] Here initial doping ($y \lesssim 0.06$) is accompanied by gradually declining line width, while an abrupt discontinuity at $y \approx 0.06$ is indicative of an electronic phase transition. Beyond this doping level, the ESR line width falls in concert with the onset of Pauli susceptibility and other metallic characteristics. As can also be seen in Table VI, the above line-width trends are essentially unaltered at 77 K. The $\{[Si(Pc)O](SO_4)_y\}_n$ ESR data deviate from the aforementioned trends in that the line widths are somewhat greater and do not fall with increasing y over the relatively narrow range that could be investigated (Figure 25, Table VI). The interpretation of this result is not unambiguous with the data at hand and further studies are in progress. The increased broadening may reflect decreased carrier mobility/greater two-dimensionality for Coulombic reasons or, alternatively, greater carrier density on the sulfate dianion and thus more efficient electronic relaxation via phonon-modulated spin–orbit interactions.[50]

(47) Mazumdar, S.; Bloch, A. N. *Phys. Rev. Lett.* **1983**, *50*, 207–211.
(48) Gutfreund, H.; Entin-Wohlman, O.; Weger, M. *Mol. Cryst. Liq. Cryst.* **1986**, *119*, 457–466, and references therein.
(49) The ESR signal at y = 0.0 can be attributed to defects and/or radical-cation sites introduced by the high-temperature polymerization process.[8b] The line width is therefore indicative of what can be expected for completely immobile spins in these systems.
(50) (a) Zuppiroli, L. In ref 3b, pp 307–333, and references therein. (b) Maresch, G. G.; Mehring, M.; von Schütz, J. U.; Wolf, H. C. *Chem. Phys.* **1984**, *85*, 333–340, and references therein.
(51) (a) Carneiro, K.; Scott, J. C.; Engler, E. M. *Solid State Commun.* **1984**, *50*, 477–481, and references therein. (b) Soos, Z.; Bondeson, S. R. In ref 3j, Vol. 3, pp 229–233. (c) Jérome, D. In *The Physics and Chemistry of Low-Dimensional Solids*; Alcacer, L., Ed.; D. Reidel: Dordrecht, The Netherlands, 1980; pp 123–142. (d) Schultz, T. D.; Craven, R. A. In *Highly Conducting One-Dimensional Solids*; Devreese, J. T., Evrard, R. P., van Doren, V. E., Eds.; Plenum Press: New York, 1979.
(52) Chen, J.; Heeger, A. J. *Synth. Met.* **1988**, *24*, 311–327.

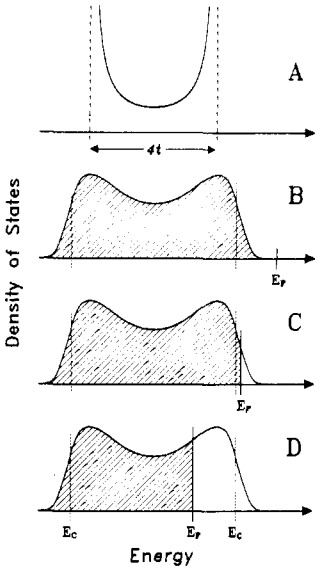

Figure 26. Schematic density of states depiction of the electronic structural consequences of electrochemically doping the cofacial polymer, tetragonal $[Si(Pc)O]_n$. A. Undoped. Classical quasi-one-dimensional tight-binding description. B. Part A in the presence of disorder and defects. C. Lightly doped. D. Heavily doped. E_F represents the Fermi energy and E_C the energy of a mobility edge.

Discussion

Response to Variations in Band Filling and Counterions. This study provides the first detailed insight into how the physical properties of a molecular metal evolve for major and continuous variations in conduction band filling. These variations are effected for relatively constant stacking and for both a small, tetrahedral, relatively nonpolarizable counterion (BF_4^-) and for a large, polarizable, flat, aromatic counterion (TOS^-). In addition, the properties of the same molecular metal are surveyed for a dinegative counterion (SO_4^{2-}). While there are clearly subtle differences in behavior as a function of counterion, the overall responses of the $\{[Si(Pc)O]X_y\}_n$ systems allow a number of important generalizations to be made.

The rather drastic changes in physical properties that occur in the vicinity of $y \approx 0.20$ indicates that a major change in electronic structure/carrier mobility occurs. The diffraction and electrochemical data[2] give no indication that equally drastic structural changes occur, but rather evidence a smooth and continuous evolution in structure as a function of y. As will be discussed below, the nature of the $y \approx 0.20$ transition is from a localized carrier, insulating material to a delocalized, low-dimensional metallike material, the properties of which continue to evolve in an instructive manner as y approaches the maximum doping stoichiometry. The electronic structural model we shall employ to describe these y-dependent changes centers around the effects of disorder and defects on the properties of a quasi-one-dimensional band structure.[26,50a,53,54] Figure 26A illustrates a density of states vs energy diagram for a classical, one-dimensional tight-binding band.[7] This is the idealized model upon which the thermoelectric power, optical spectroscopic, and magnetic relationships of eq 6 (Figure 15), 10, and 13 (Figure 24), respectively, are based. The effect on this band structure of disorder and defects will be to alter the density of states as shown schematically in Figure 26B and to introduce a mobility edge (E_C) interposed between localized states at the tails of the band and the more central, delocalized (metallike) states.[26,50a,53,54] A transition of the Fermi level (E_F) across such an edge as a function of composition or some other property is classically known as an Anderson transition.[53]

At low oxidation (y) levels, it appears likely that the doped polymer is significantly disordered, presumably as a consequence of varying $[Si(Pc)O]_n$ chain lengths and/or crystallographic positions (implicated in electron microscopy studies[55]) as well as possibly other types of defects (including disorder and/or clustering in anion locations). The result of these perturbations will be localization of conduction band states at the tails of the band. In this type of regime, the carriers (holes) will therefore have low mobilities. The charge-transport data are in good accord with this model: the dc conductivity is low, exhibits high apparent activation energies (as polycrystalline specimens), and can be fit to a model appropriate for disordered systems or one-dimensional carrier hopping between localized states (Figures 8–10). At this same doping level, the magnitude and temperature dependence of thermoelectric power is also typical of a p-type semiconductor (Figures 12–14). Further evidence for carrier localization in this regime is seen in the optical reflectivity, which is in accord with a semiconducting or insulating electronic structure (Figures 16 and 17), and the magnetic susceptibility, which evidences a high concentration of localized Curie-like spins and little, if any, Pauli-like character (Figure 23).[56] Furthermore, the ESR line width is also suggestive of less mobile spins.

In the region of $y \approx 0.20$, major changes are detected in the $\{[Si(Pc)O]X_y\}_n$ electronic structure and transport characteristics. Both the magnitude and temperature dependence of the thermoelectric power evidence a transition to a metallike substance (Figures 12 and 13). While interparticle contact effects likely damp out the sharpness of the transition, the electrical conductivity begins to level off in the vicinity of $y \approx 0.20$ while the apparent activation energies (slopes in log σ vs T) fall (Figures 2 and 3). Coincidentally, the stoichiometric location of this insulator-to-metal transition is near the percolation threshold for inhomogeneously (chemically) doped $[Si(Pc)O]_n$.[8] For $y \gtrsim 0.20$, the temperature dependence of the conductivity of the present materials can be better fit to a fluctuation-induced tunneling transport model appropriate for a more metallike material (Figures 5 and 6).[8] Also at $y \approx 0.20$, a metallike plasma edge is first observed in the optical reflectivity (Figures 16 and 17), while magnetic measurements indicate that the concentration of Curie-like spins drops precipitously and the concentration of Pauli-like (metallike) spins sharply rises. ESR line widths exhibit a decrease (more discontinuous for $\{[Si(Pc)O](BF_4)_y\}_n$) to values characteristic of more mobile spins. In terms of the model shown in Figure 26, the $y \approx 0.20$ doping region represents the point at which the Fermi level has crossed the mobility edge. This picture represents a marked contrast to a classical model (Figure 26A), which predicts a "turn-on" of metallic characteristics at the lowest doping levels. To our knowledge, such a "turn-on" has never been observed in a low-dimensional molecular metal.[3]

Emptying of the band structure beyond $y \approx 0.25$ evokes a number of interesting responses. The room-temperature electrical conductivity remains remarkably constant over a very broad range (Figure 1), while the decrease in apparent activation energy is

(53) (a) Mott, N. F. *Conduction in Non-Crystalline Materials*; Clarendon Press: Oxford, 1987; Chapters 2, 3. (b) Mott, N. F. *Metal-Insulator Transitions*; Taylor and Francis: London, 1974; Chapters 1, 6. (c) Berezinskii, V. L. *Sov. Phys.-JETP (Engl. Transl.)* **1974**, *38*, 620–627. (d) Anderson, P. W. *Phys. Rev.* **1958**, *109*, 1492–1505.

(54) In a *rigorously* one-dimensional chain, disorder will lead to localization of *all* states, and conduction can only occur via phonon-assisted hopping.[53b,54a,b] To our knowledge, such a high degree of unidimensionality has not been physically achieved, and all known molecular metals exhibit significant two- or three-dimensional character. (a) Bloch, A. N.; Wilson, R. B.; Varma, C. M. *Phys. Rev. Lett.* **1972**, *28*, 753–756. (b) Mott, N. F. *Adv. Phys.* **1967**, *16*, 49–144.

(55) (a) Zhou, X.; Marks, T. J.; Carr, S. H. *Mol. Cryst. Liq. Cryst.* **1985**, *118*, 357–360. (b) Zhou, X.; Marks, T. J.; Carr, S. H. *J. Polym. Sci., Polym. Phys. Ed.* **1985**, *23*, 305–313. (c) Zhou, X.; Marks, T. J.; Carr, S. H., manuscript in preparation.

(56) (a) Classical Anderson localization is predicted to give rise to a "Fermi-glass" electronic structure with a relatively continuous density of localized states.[53] The magnetic properties of such a system are predicted to be Curie-like at lower temperatures and less temperature-dependent at high temperatures.[56b] The reflectivity will not be strictly Drude-like and should exhibit significant drop-off at lower frequencies.[54b] (b) Wudl, F.; Angus, R. O., Jr.; Lu, F. L.; Allemand, P. M.; Bachon, D. J.; Novak, M.; Liu, Z. X.; Heeger, A. J. *J. Am. Chem. Soc.* **1987**, *109*, 3677–3684, and references therein.

smaller than in the $y \approx 0.20$ region (Figures 3 and 4). Beyond $y \approx 0.35$, the Pauli-like component of the static magnetic susceptibility remains nearly constant while the Curie-like component falls to a low, constant level. Meanwhile, the ESR line widths fall to levels typical of unidimensional phthalocyanine molecular metals not having heavy-atom counterions[8a] (i.e., where relaxation processes involving phonon modulation of spin–orbit coupling do not greatly broaden the lines). For y increasing beyond ca. 0.25, the optical plasma edge shifts continuously to higher energy, in good accord with simple tight-binding band theory (Figure 20). These observations are in general agreement with the description of Figure 26D in which the Fermi level is in the metallic portion of the conduction band and in which the density of states varies only modestly as a function of y. The latter point is especially argued by the weak sensitivity of the conductivity and Pauli-like susceptibility to changes in y. As noted earlier, agreement between observables, such as bandwidths calculated from a simple tight-binding analysis of thermopower and optical reflectivity data and those estimated by other methods,[39] is always poor at low doping levels, but satisfactory at higher ($\rho \approx +0.25$ to $+0.67$) doping levels. Comparison of part A of Figure 26 to parts B–D shows that the reason resides principally in how the density of states responds to disorder and defects. The deviation of the actual density of states from the idealized model (Figure 26A) upon which eq 6, 10, and 13 are based is clearly greatest near the tails of the band, i.e., at low and very high (not yet realized) doping levels.

The optical and especially thermoelectric power data underscore the differences between the $\{[Si(Pc)O](BF_4)_y\}_n$ and $\{[Si(Pc)O](TOS)_y\}_n$ materials. The optical data reveal slightly lower bandwidths for the TOS^--containing polymers (Table IV) which are also in accord with the slightly higher Pauli-like static magnetic susceptibilities (Table V). A reasonable explanation may be reduced Pc–Pc ring overlap arising from the disorder in the TOS^- packing (suggested by the diffraction data[2]) and displacement of Pc–Pc eclipsing angles from optimum overlap.[39e] The variable-temperature thermoelectric power data evidence differences between the BF_4^-- and TOS^--containing materials and also deviations from behavior expected in a simple one-dimensional tight-binding picture (Figure 15). The latter picture predicts, for $U = 0$ and energy-independent scattering, no change in sign until $\rho = +1.0$. The theoretical description is, of course, far more intricate and less well developed when Coulombic, electron–electron repulsive interactions are introduced.[33,34,38] However, it is noteworthy that neither the static susceptibilities nor electrical conductivities of the present materials are suggestive of very large U systems ($U \gg 4t$, recognizing, of course, that U is doubtless ρ-dependent[45a,47]), nor does the thermopower at $y \approx 0.50$ exhibit the temperature-independent, $|S| \approx 60\ \mu V/K$ behavior frequently observed for large U systems where the upper Hubbard band is half-filled.[33,36] Clearly off-axis counterions of grossly different shapes, sizes, and polarizabilities do perturb the $[Si(Pc^{\rho+})O]_n$ band structure to some degree.

Band structure–counterion interactions were also probed with the tetrahedral, dinegative gegenion, SO_4^{2-}. Although the intrinsic redox properties of SO_4^{2-} limit the maximum doping level to $y \approx 0.19$, the charge-transport, optical, and magnetic measurements give no evidence of unusual localization or carrier trapping effects with the possible exception of slightly broadened ESR line shapes. It is likely that the structure-enforcing nature of the $(-SiO-)_n$ chain and the resulting enforced Pc–Pc cofaciality is a major factor here.

Comparison to Other Molecular and Polymeric Conductors. It is instructive at this point to contrast the present results with the rather different pictures that have emerged for other conductive molecular and polymeric materials in which tuning of the oxidation level has been possible. The band filling in the low-dimensional molecular conductor $(NMP)_x(Phen)_{1-x}(TCNQ)$, where NMP = *N*-methylphenazine and Phen = phenazine, can be tuned from $\rho \approx -0.50 \rightarrow -0.66$ in the TCNQ stack by substitution of neutral Phen for NMP^+.[57] Electron–phonon coupling is very large in this system, giving rise to a Peierls distortion in the stacking architecture[57,58] and gap-related semiconducting transport behavior even at room temperature. As x is varied from 1.0 to 0.5, the material changes (at $x \approx 0.65$) from a two-chain conductor with a relatively small U (and a $2k_F$ stacking distortion) to a large U single-chain (TCNQ) conductor (having a $4k_F$ stacking distortion). In the narrow region $x \approx 0.50$–0.56, excess charge is accommodated by maintaining a commensurate (dimerized) TCNQ stacking architecture and forming charged pairs of soliton defects (bipolarons).[57] This behavior is to be contrasted with phthalocyanine conductors, where $M(Pc)X_y$ systems exhibit metallic characteristics and no evidence of a Peierls instability down to lowest temperatures,[5] and where the lattice-stiffening of the $\{[Si(Pc)O]X_y\}_n$ backbone and the lower bandwidth are likely to further oppose electron–phonon coupling-based structural distortions. In addition, off-axis counterion screening effects (e.g., the $2k_F \rightarrow 4k_F$ crossover) appear to be far larger in the $(NMP)_x(Phen)_{1-x}(TCNQ)$ systems.[57]

$\{[Si(Pc)O]X_y\}_n$ conductors differ from the great majority of electrically conductive polymers in that the conjugation pathway does not coincide with the apparent charge-transport pathway and electron–phonon coupling is much smaller. Thus, initial doping of Peierls-distorted[7] *trans*-polyacetylene results in a decrease in the magnetic susceptibility and semiconducting transport via spinless charged soliton defects.[23a,59] At the doping level of ca. $[(CH)X_{0.06}]_n$, there is an abrupt transition to a metallic state with Pauli-like magnetic susceptibility. At this point, the material has been described as a polaron metal[59] or as having a disorder-induced metallic density of states in the Peierls gap.[60] Polyacetylene can be prepared in highly crystalline microstructures, considerable crystal structure-doping information exists, and off-axis counterion effects are being explored.[59,61] There is far less structural information on polypyrrole and polyaniline. Both have nondegenerate ground states and strong electron–phonon coupling. Incremental doping of the former material gives rise initially to polarons, then predominantly to spinless bipolarons.[62] Thus, the magnetic susceptibility initially increases, goes through a broad maximum, and then drops to very low levels as doping progresses ($0.0 \rightarrow 0.33$ holes/monomer unit). The magnitude of the susceptibility is never Pauli-like. The conductivity peaks near the maximum in the susceptibility and then remains approximately constant. The temperature dependence at all doping levels is suggestive of carrier hopping between localized states. To our knowledge, the homogeneity and crystal structural aspects of polypyrrole doping remain obscure. Doping (via protonation) of polyaniline[32,63] is believed to be largely inhomogeneous using the type of $\chi(y)$ arguments originally used for $\{[Si(Pc)O]I_y\}_n$ (cf. Figure 23).[5b] The properties of the fully doped material have been described both as a granular polaronic metal above the percolation threshold[32] and as a nonmetallic "Fermi glass".[56b] A number of aspects of the undoped and doped polyaniline macromolecular structures are at present unresolved.

(57) (a) Miller, J. S.; Epstein, A. J. *Angew. Chem., Int. Ed. Engl.* **1987**, *26*, 287–293. (b) Javadi, H. H. S.; Miller, J. S.; Epstein, A. J. *Phys. Rev. Lett.* **1987**, *59*, 1760–1763. (c) Conwell E. M.; Howard, I. A. *Phys. Rev. B.* **1985**, *31*, 7835–7843. (d) Epstein, A. J.; Kaufer, J. W.; Rommelmann, H.; Howard, I. A.; Conwell E. M.; Miller, J. S.; Pouget, J. P.; Comis, R. *Phys. Rev. Lett.* **1982**, *49*, 1037–1041.

(58) Epstein, A. J.; Miller, J. S.; Pouget, J. P.; Comês, R. *Phys. Rev. Lett.* **1981**, *47*, 741–744.

(59) (a) Chen, J.; Heeger, A. J. *Synth. Met.* **1988**, *24*, 311–327. (b) Heeger, A. J. In *Handbook of Conducting Polymers*; Skotheim, T. A., Ed.; Marcel Dekker: New York, 1986; Vol. 1, 2, Chapter 21, and references therein. (c) Kivelson, S.; Heeger, A. J. *Phys. Rev. Lett.* **1985**, *55*, 308–311.

(60) (a) Yang, X. Z.; Tanner, D. B.; Rice, M. J.; Gibson, H. W.; Feldblum, A.; Epstein, A. J. *Solid State Commun.* **1987**, *61*, 335–340. (b) Mele, E. J.; Rice, M. J. *Phys. Rev. B* **1981**, *23*, 5397–5412. (c) Conwell, E. M.; Jeyadev, S. *Synth. Met.* **1979**, *28*, D489–D494, and references therein.

(61) (a) Winokur, M.; Moon, Y. B.; Heeger, A. J.; Barker, J.; Bott, D. C.; Shirakawa, H. *Phys. Rev. Lett.* **1987**, *58*, 2329–2332. (b) Moon, Y. B.; Winokur, M.; Heeger, A. J.; Barker, J.; Bott, D. C. *Macromolecules* **1987**, *20*, 2457–2461.

(62) (a) Street, G. B. In ref 59b, Chapter 8. (b) Pfluger, P.; Weiser, G.; Scott, J. C.; Street, G. B. In ref 59b, Chapter 38. (c) Genoud, F.; Guglielmi, M.; Nechtschein, M.; Genies, E.; Salmon, M. *Phys. Rev. Lett.* **1985**, *55*, 118–121.

(63) Ginder, J. M.; Richter, A. F.; MacDiarmid, A. G.; Epstein, A. J. *Solid State Common.* **1987**, *63*, 97–101.

Conclusions

In concert with the electrochemical and structural results,[2] the present work provides what is perhaps the most complete picture to date of how the collective properties of a molecular metal with structure-enforced stacking respond to fairly drastic changes in off-axis counterions and band filling. It is seen that subtle counterion effects on the band structure are operative and appear at this state to be largely structural in origin. However, these effects are of a considerably lesser magnitude than observed in typical molecular metals such as $(TMTSF)_2X$, $(BEDT\text{-}TTF)_2X$, etc., where major structural and, consequently, electrical, optical, and magnetic changes accompany variations in X^-.[3] The response of $[Si(Pc^{\rho+})O]_n$ collective properties to major excursions in ρ is largely understandable in terms of simple tight-binding band theory, however, only if the effects of disorder and defects are taken into account. Such effects are particularly pronounced at low $\rho+$ values.

Acknowledgment. This research was supported by the NSF through the Northwestern Materials Research Center (Grant DMR 85202280) and by the Office of Naval Research. M.A. thanks NATO for a postdoctoral fellowship.

Supplementary Material Available: Plots of $\{[Si(Pc)O]X_y\}_n$ conductivity data according to fluctuation-induced tunneling and variable range hopping transport models (5 pages). Ordering information is given on any current masthead page.

Metal Alkoxides. Models for Metal Oxides. 15.[1] Carbon–Carbon and Carbon–Hydrogen Bond Activation in the Reactions between Ethylene and Ditungsten Hexaalkoxides: $W_2(OCH_2\text{-}t\text{-}Bu)_6(\eta^2\text{-}C_2H_4)_2$, $W_2(OR)_6(CH_2)_4(\eta^2\text{-}C_2H_4)$, and $W_2(OR)_6(\mu\text{-}CCH_2CH_2CH_2)$ (Where R = $CH_2\text{-}t\text{-}Bu$, *i*-Pr, c-C_5H_9, and c-C_6H_{11}). Preparations, Properties, Structures, and Reaction Mechanisms

Malcolm H. Chisholm,* John C. Huffman, and Mark J. Hampden-Smith

Contribution from the Department of Chemistry and Molecular Structure Center, Indiana University, Bloomington, Indiana 47405. *Received September 1, 1988*

Abstract: $W_2(OR)_6(M{\equiv}M)$ compounds and ethylene (1 atm, 22 °C) react in alkane and aromatic hydrocarbon solvents to give $W_2(OR)_6(\mu\text{-}CCH_2CH_2CH_2)$ compounds and ethane, where R = *i*-Pr, c-C_5H_9, c-C_6H_{11}, and $CH_2\text{-}t\text{-}Bu$. Under comparable conditions, $W_2(O\text{-}t\text{-}Bu)_6$ and ethylene fail to react. In the formation of $W_2(OR)_6(\mu\text{-}CCH_2CH_2CH_2)$ compounds, the intermediates $W_2(OCH_2\text{-}t\text{-}Bu)_6(\eta^2\text{-}C_2H_4)_2$ and $W_2(OR)_6(CH_2)_4(\eta^2\text{-}C_2H_4)$, where R = c-$C_5H_9$, *i*-Pr, and $CH_2\text{-}t\text{-}Bu$, have been characterized. For R = *i*-Pr and $CH_2\text{-}t\text{-}Bu$, the intermediates are shown to be formed *reversibly* from $W_2(OR)_6$ and ethylene. The compound $W_2(O\text{-}i\text{-}Pr)_6(CH_2)_4(\eta^2\text{-}C_2H_4)$ has been fully characterized by an X-ray study and found to contain a metallacyclopentane ring and a $W\text{-}\eta^2\text{-}C_2H_4$ moiety, one at each metal center. The pyridine adduct $W_2(O\text{-}i\text{-}Pr)_6(\mu\text{-}CCH_2CH_2CH_2)(py)$ has been fully characterized and shown to contain a novel 1,6-dimetallabicyclo[3.1.0]hex-1(5)-ene organometallic core. All compounds have been characterized by ^{13}C and ^1H NMR studies. Various aspects of the reaction pathway have been probed by the use of isotopically labeled ethylenes, and a proposed general scheme is compared to previous studies of ethylene activation at mononuclear metal centers and carbonyl dinuclear and cluster compounds. Crystal data for $W_2(O\text{-}i\text{-}Pr)_6(\mu\text{-}CCH_2CH_2CH_2)(py)\cdot{}^1/_2py$ at −150 °C: a = 10.968 (2) Å, b = 17.507 (4) Å, c = 9.433 (1) Å, α = 93.56 (1)°, β = 96.83 (1)°, γ = 101.29 (1)°, Z = 2, d_{calcd} = 1.693 g cm^{-3}, space group $P\bar{1}$. For $W_2(O\text{-}i\text{-}Pr)_6(CH_2)_4(\eta^2\text{-}C_2H_4)$ at −155 °C: a = 10.069 (2) Å, b = 17.033 (9) Å, c = 17.278 (9) Å, β = 91.38 (3)°, Z = 4, d_{calcd} = 1.808 g cm^{-3}, space group = $P2_1/c$.

Organotransition-metal chemistry has largely evolved through the use of soft π-acceptor ligands such as carbon monoxide, tertiary phosphines, and $\eta^x\text{-}C_n$ ligands (olefins, dienes, allyl, cyclopentadienyl, arenes, etc.).[2,3] Synthetic and mechanistic aspects of organometallic chemistry have been transported from one area of the periodic table to another in a ligand-dependent approach. The ubiquitous Cp and Cp* ligands (Cp = $\eta^5\text{-}C_5H_5$, Cp* = $\eta^5\text{-}C_5Me_5$) have, within the last decade, been key to important developments in the chemistry of the early transition elements,[4,5] the lanthanides and actinides,[6,7] as well as various later transition[8] and main-group elements.[9] In other instances the existence of metal cluster carbonyl compounds has allowed the reactivity of hydrocarbyl fragments to be investigated as a function of multimetal site attachment.[10] Often striking analogies in bonding modes are seen for hydrocarbyl fragments in metal carbonyl cluster compounds and metal surface chemistry.[11]

(1) Chisholm, M. H.; Folting, K.; Huffman, J. C.; Klang, J. A.; Streib, W. E. *Organometallics* **1989**, *8*, 89.
(2) Coates, G. E.; Green, M. L. H.; Wade, K. *Organometallic Compounds: The Transition Elements*, 3rd ed.; Methuen: London, 1968.
(3) Collman, J. P.; Hegadus, L. S.; Norton, J. R.; Finke, R. G. *Principles and Applications of Organotransition Metal Chemistry*; University Science Books: Mill Valley, CA, 1987.
(4) Bercaw, J. E.; Wolczanski, P. T. *Acc. Chem. Res.* **1980**, *13*, 121.
(5) Bercaw, J. E.; Thompson, M. E. *Pure Appl. Chem.* **1984**, *56*, 1.
(6) Evans, W. J. *Adv. Organomet. Chem.* **1985**, *24*, 131; *Polyhedron* **1987**, *6*, 803.
(7) *Fundamental and Technological Aspects of Organo-f-Element Chemistry*; Marks, T. J., Fragala, I. L., Eds.; NATO ASI Series, Series C; D. Reidel: Dordrecht, The Netherlands, 1985; No. 155.
(8) (a) Bergman, R. G. *Science* **1984**, *223*, 902. (b) Herrmann, W. A. *Polyhedron* **1987**, *6*, 1165.
(9) Jutzi, P. *Adv. Organomet. Chem.* **1986**, *26*, 217.
(10) Chisholm, M. H., Ed. Reactivity of Bridging Hydrocarbyl Ligands. Polyhedron Symposium in Print No. 4 *Polyhedron* **1987**, *7*(10/11).

0002-7863/89/1511-5284$01.50/0